

LitFM: A Retrieval Augmented Structure-aware Foundation Model For Citation Graphs

Jiasheng Zhang¹, Jialin Chen², Ali Maatouk², Ngoc Bui²,
 Qianqian Xie², Leandros Tassioulas², Jie Shao¹, Hua Xu², and Rex Ying²
¹University of Electronic Science and Technology of China ²Yale University
 zjss12358@std.uestc.edu.cn, shaojie@uestc.edu.cn

{jialin.chen, ali.maatouk, ngoc.bui, qianqian.xie, leandros.tassioulas, hua.xu, rex.ying}@yale.edu

Abstract

With the advent of large language models (LLMs), managing scientific literature via LLMs has become a promising direction of research. However, existing approaches often overlook the rich structural and semantic relevance among scientific literature, limiting their ability to discern the relationships between pieces of scientific knowledge, and suffer from various types of hallucinations. These methods also focus narrowly on individual downstream tasks, limiting their applicability across use cases. Here we propose LitFM, the first literature foundation model designed for a wide variety of practical downstream tasks on domain-specific literature, with a focus on citation information. At its core, LitFM contains a novel graph retriever to integrate graph structure by navigating citation graphs and extracting relevant literature, thereby enhancing model reliability. LitFM also leverages a knowledge-infused LLM, fine-tuned through a well-developed instruction paradigm. It enables LitFM to extract domain-specific knowledge from literature and reason relationships among them. By integrating citation graphs during both training and inference, LitFM can generalize to unseen papers and accurately assess their relevance within existing literature. Additionally, we introduce new large-scale literature citation benchmark datasets on three academic fields, featuring sentence-level citation information and local context. Extensive experiments validate the superiority of LitFM, achieving 28.1% improvement on retrieval task in precision, and an average improvement of 7.52% over state-of-the-art across six downstream literature-related tasks.

Introduction

The rapid expansion of scientific literature necessitates effective management and analysis for scientific research (Sun et al. 2024; Tsai et al. 2023; Luo, Xie, and Ananiadou 2023). Traditional approaches rely primarily on rule-based or statistic-based methods (Liu, Zhang, and Guo 2013), showing inherent limitations in their capabilities. Due to the enhanced semantic understanding of large language models (LLMs), recent efforts have attempted to use LLMs to manage literature through human instructions (Zhang et al. 2023a; Shen et al. 2024; Baek et al. 2024).

Despite their advancements, these models typically overlook the interconnected nature and structural relevance of citation graphs. This negligence limits their ability to fully comprehend both individual research papers and the broader

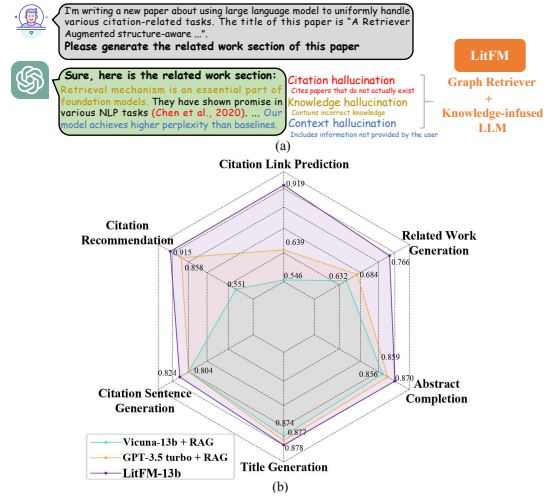


Figure 1: (a) Hallucinations faced by existing approaches. (b) Performance of LitFM and existing approaches on six benchmark tasks, where LitFM shows consistent superiority.

academic context in which they exist. Consequently, these models suffer from several limitations: **1) Hallucinations.** They often overlook the use of citation graphs or fail to grasp the nuanced semantics of paper-to-paper citations. As shown in Figure 1(a), this oversight leads to responses that exhibit hallucinations in citation, knowledge, and context for a given input (Kunnath, Pride, and Knoth 2023; Martin-Boyle et al. 2024). In this regard, citation hallucination refers to the citing of non-existent literature, knowledge hallucination involves providing information that contradicts the actual literature, while context hallucination means including information that was neither provided nor desired by the user. **2) Generalization ability.** Existing methods heavily rely on the accessibility to the complete context of the given text and struggle to handle unseen topics or research texts with incomplete information. This dependency significantly restricts their applicability and adaptability (Li and Ouyang 2024a). **3) Unification.** Current approaches to enhance literature-related capabilities often focus on specific tasks. This narrow focus neglects the potential for LLMs to transfer knowledge across different tasks (Luo, Xie, and Ananiadou 2023; Yang and Han 2023), which is particularly pronounced in complex tasks such as related work genera-

tion (Li and Ouyang 2024b).

Proposed Works. To address these challenges, we propose **LitFM**, the first **L**iterature **F**oundation **M**odel¹ designed to uniformly manage diverse literature-related tasks using domain-specific citation graphs. To avoid citation hallucinations, we design a structure-aware retriever to extract literature from citation graphs as references. Different from existing graph-based retrieval methods (He et al. 2024), which often overlook neighboring information, our graph retriever integrates structural details through neighbor-aware candidate embeddings. Additionally, we implement a self-supervised pre-training that adapts the graph retriever to the specific semantic and structural features of the citation graph. To enhance the generalization ability of our framework, we introduce a novel notion of pseudo-query that encourages the retriever to generate embeddings that mirror a complete query in both semantic and structural aspects, thereby enhancing reliability in challenging scenarios where the input query may be incomplete or contain unseen topics.

To unify various literature-related tasks while infusing domain-specific knowledge to avoid knowledge hallucinations, we introduce an instruction-tuning paradigm for citation graph understanding. By fine-tuning the LLM through this paradigm using real-world citation graphs, the LLM learns to extract intrinsic knowledge, essential arguments, and relations between the scientific literature. This approach not only unifies task handling but also enhances the LLM’s knowledge transferability across tasks, resulting in overall improved performance. Using a chain-of-thought (COT) (Wei et al. 2022) strategy, we demonstrate that LitFM can automatically generate literature reviews for papers outside the existing citation graph, effectively avoiding fake citations and providing more informative content.

To construct the instruction and benchmark dataset, we curate and open-source three new citation graph datasets, covering diverse domains². While there are existing citation graph datasets in the literature, such as ogbn-arxiv-TA (Yan et al. 2023) and Semantic Scholar Network dataset (An et al. 2021), they are either limited in scale (e.g., the ogbn-arxiv-TA dataset only contains 1M edges) or lack detailed context for each citation edge (e.g., only the text descriptions of nodes are provided). Instead, our new datasets are augmented with fine-grained citation sentences describing where the citation occurs and their local context. This local context helps better understand the intent behind the citation and facilitates a more accurate interpretation of citation relations. Moreover, nodes are enriched with related work sections as attributes, providing a valuable test bed for evaluating the quality of tasks such as related work generation.

We conducted experiments on 6 real-world literature-related tasks, with results reported in Figure 1(b). As shown in the figure, LitFM outperforms retriever-augmented GPT-3.5-turbo across all tasks. Particularly, LitFM surpasses GPT-3.5-turbo by 32.8% and 8.3% in citation prediction and citation recommendation tasks, respectively. This performance boost is attributed to the high fidelity of our graph

retriever, which achieves 28.1% higher precision in retrieving related literature compared to existing retrieval baselines. Finally, our zero-shot evaluation on the related work generation task shows that LitFM attains a 17.8% higher ROUGE score than GPT-3.5-turbo with more accurate citations and produces text that more closely aligns with the statistical distribution of ground-truth related-work sections.

Related Work

Deep Learning on Citation Graphs. Citation graphs are extensively utilized in numerous research studies (Zhang et al. 2023c). Early works have applied traditional machine learning model (Hamilton, Ying, and Leskovec 2017) for citation graph analysis and recommendation (Iqbal et al. 2021; Ali et al. 2020). However, they are often designed for a specific task, lacking a unified model that performs well across different tasks. Efforts such as SciBERT (Beltagy, Lo, and Cohan 2019), BioBERT (Lee et al. 2020), PubMedBERT (Gu et al. 2021), SciMult (Zhang et al. 2023a) aim for general understanding of scientific literature but are only applicable for discriminative tasks due to their emphasis on representation learning. Recent works (Jung et al. 2023; Martin-Boyle et al. 2024; Li and Ouyang 2024b) leverage LLMs to enable generation tasks but are typically designed for specific tasks. Further, they often separate training from real citation graphs, limiting adaptability to network dynamics.

Large Language Models for Graphs. Existing strategies for leveraging LLMs in graph learning (Minaee et al. 2024; Ren et al. 2024) include using GNNs as encoders to convert graph entities into structure-aware tokens for LLM inference (Tang et al. 2024a; Chai et al. 2023), or using LLMs as text encoders for node embeddings to train GNNs (Huang et al. 2023; Xia, Kao, and Huang 2024; Chen et al. 2023) or fused GNN-LLM models (Li, Ding, and Lee 2023; Huang et al. 2024). Another branch involves retrieving and translating subgraphs into text for inference (He et al. 2024; Hu et al. 2024), with fine-tuning to improve LLM understanding of subgraph context (Zhao et al. 2023; Fatemi, Halcrow, and Perozzi 2023; Chen et al. 2024a; Luo et al. 2024).

Retrieval Augmented Generation (RAG). Vanilla LLMs commonly face challenges like hallucinations (Zhang et al. 2023b), outdated knowledge (Zhang et al. 2023d), and uninterpretable reasoning process (Jie et al. 2024; Tang et al. 2024b) in domain-specific or knowledge-intensive tasks. RAG addresses these issues by incorporating external knowledge as additional context to improve LLM performance (Gao et al. 2023). Originating from language applications, most of the current work on RAG for LLMs is on textual data gathered from one or multiple corpuses (Gao et al. 2023; Zhao et al. 2024). Several later attempts adapt these approaches for (semi-) structural data such as tabular data (Luo et al. 2023; Zha et al. 2023), knowledge graphs (Kang et al. 2023; Wang et al. 2023; Shen et al. 2023; Jiang et al. 2024; He et al. 2024). He et al. (2024) is the closest work to ours that enhances graph question-answering capabilities by extracting subgraphs based on the retrieved nodes. However, it ignores the structural dependency during retrieval. Hence, these methods fail to achieve accurate re-

¹<https://anonymous.4open.science/r/LitFM-5EB3>

²Datasets will be made public in the camera-ready version.

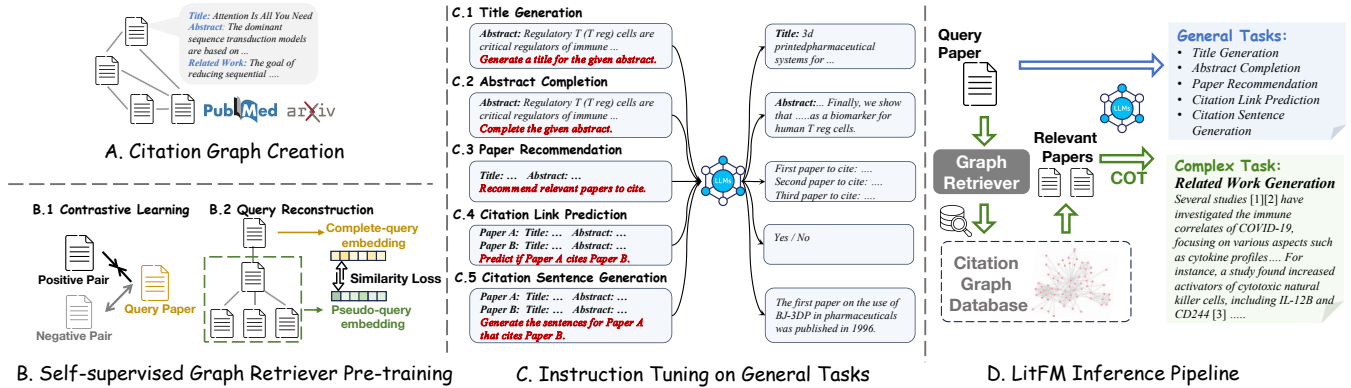


Figure 2: Main components of LitFM consists (A) The first citation graph benchmark datasets with enriched citation context, based on which the domain-specific citation instruction tuning sets are constructed. (B) Neighbor-aware graph retriever with pseudo-query embedding. The self-supervised pre-training is employed to adapt the graph retriever to the domain properties. (C) Instruction paradigm for citation graph understanding, which infuses domain-specific knowledge into LLMs. (D) The retriever-augmented pipeline that can uniformly manage various literature-related tasks.

trieval for scientific literature due to neglecting the semantic and structural relevance of literature.

Methodology

Problem Formulation. Our overarching goal is to develop a literature foundational model that can effectively address various literature-related tasks commonly encountered in real-world scientific research. These tasks include, for example, generating a title from a paper’s abstract, completing an abstract, and creating a related works section specific to domains such as medicine and physics. To achieve this, we define x as the user query related to these tasks. A citation graph $\mathcal{G} = (V, E)$ specific to the domain of interest is available, where each node $i \in V$ represents a paper, and edges E denote citation relationships between papers. Our method LitFM produces an output y to address the query x by 1) navigating \mathcal{G} and extracting literature relevant to x , 2) leveraging pseudo-query embedding to handle cases where x contains incomplete information or requires access to sparsely connected papers in \mathcal{G} , and 3) internalizing various tasks and aligning domain-specific knowledge through a unified instruction paradigm.

Method Overview. Figure 2 illustrates LitFM’s pipeline, detailing its components and steps. This includes the creation of citation graphs for training and evaluation, a self-supervised graph retriever pre-training using a contrastive framework with complete and pseudo-queries for retrieving relevant papers, an instruction paradigm to integrate various tasks and literature knowledge, and an inference process employing a chain-of-thought strategy to address complex tasks like generating related work sections. We detail these components in the following sections.

Graph Retriever

Citation graphs from different domains often exhibit various structural and semantic properties (e.g., citation preferences and terminology). Modeling these properties is essential for accurate retrieval. However, existing RAG meth-

ods (He et al. 2024) generally do not address these domain-specific aspects and often fail to incorporate neighboring information during retrieval, leading to unsatisfactory retrieval quality. To address this, our graph retriever is pre-trained using self-supervision to adapt to each research domain. We propose the novel notion of pseudo-query embedding and neighbor-aware modeling to integrate the semantic and structural dependencies among literature. With our graph retriever, LitFM can scale to citation contexts that exceed the input window limitation and extract accurate literature references to reduce hallucinations. It comprises three main steps: indexing, self-supervised training, and retrieval.

Indexing. We initiate the retriever by generating embeddings for the literature. For a paper $i \in \mathcal{G}$, let T_i and A_i denote its title and abstract. The embedding for node i is defined as $\mathbf{z}_i = LM(T_i) + LM(A_i) \in \mathbb{R}^d$, where d denotes the embedding dimension and LM refers to the pre-trained language model, such as BERT (Devlin et al. 2019).

Self-supervised Training. Connections in citation graphs indicate the semantic and structural relevance among literature, which is essential for understanding the domain properties. Therefore, we propose a self-supervised training process requiring the model to reconstruct connections between literature. Specifically, we first randomly select paper i from the citation graph as the query paper and generate the query embedding as $\mathbf{q}_i = \mathbf{W}^q \mathbf{z}_i + \mathbf{b}^q \in \mathbb{R}^{d_1}$, where $\mathbf{W}^q \in \mathbb{R}^{d_1 \times d}$ and $\mathbf{b}^q \in \mathbb{R}^{d_1}$ are trainable parameters, and d_1 indicates the hidden dimension. Then, the papers with connections to i are regarded as positive candidates and the other ones as negative. The embedding of a candidate paper j is generated by aggregating embeddings of neighborhood papers with one message passing layer (Gilmer et al. 2017)

$$\mathbf{c}_j = \mathbf{W}^{c1} \mathbf{z}_j + \frac{1}{|\mathcal{N}(j)|} \sum_{k \in \mathcal{N}(j)} \mathbf{W}^{c2} \mathbf{z}_k + \mathbf{b}^c \in \mathbb{R}^{d_1}, \quad (1)$$

where $\mathcal{N}(j)$ is the neighborhood papers of j . $\mathbf{W}^{(\cdot)} \in \mathbb{R}^{d_1 \times d}$ and $\mathbf{b}^c \in \mathbb{R}^{d_1}$ are learnable during training. Integrating neighborhood information helps the retriever consider the

broader context of each paper, thereby enhancing the quality and diversity of the retrieval results.

In practical usage, user-provided queries may be incomplete (e.g., partial titles or fragmented sentences). To handle these incomplete queries, we further introduce pseudo-query embeddings. Our graph retriever reconstructs an embedding for the complete query, known as the pseudo-query embedding, based on each candidate. This allows us to use the similarity between the embeddings of user-provided query and pseudo query as an auxiliary metric during retrieval. Since our goal is to retrieve the related papers for a given paper, each pair of connected papers (i.e., $(i, j) \in E$) in the citation graph can be regarded as a ground-truth query-candidate match, where the text of the source node i serves as the complete query for the text of the target node j . Therefore, we first use a multilayer perceptron (MLP) to generate the pseudo-query embedding from candidate paper j as $\mathbf{p}_j = \text{MLP}(\mathbf{c}_j) \in \mathbb{R}^{d_1}$, and then employ the 1-norm regularization to ensure that the pseudo-query embedding closely resembles the embedding of paper i , as shown in Eq. 2:

$$\mathcal{L}_{\text{re}} = \sum_{(i,j) \in \mathcal{G}} \|\mathbf{z}_i - \mathbf{p}_j\|_1. \quad (2)$$

Given the candidate embedding \mathbf{c}_j and the pseudo-query embedding \mathbf{p}_j , we calculate the cosine similarity between the query and the candidate as $\text{sim}(i, j) = \cos(\mathbf{q}_i, \mathbf{c}_j + \mathbf{p}_j)$. We then apply the InfoNCE loss (Oord, Li, and Vinyals 2018) to ensure positive candidates are closer to the query embeddings than negative candidates in the semantic space:

$$\mathcal{L}_{\text{ncc}} = -\frac{1}{|\mathcal{N}(i)|} \sum_{j \in \mathcal{N}(i)} \log \frac{\exp(\text{sim}(i, j))}{\sum_{j' \notin \mathcal{N}(i)} \exp(\text{sim}(i, j'))}, \quad (3)$$

where the negative candidates j' are randomly sampled from $V \setminus \mathcal{N}(i)$. We then optimize the retriever with the InfoNCE loss \mathcal{L}_{ncc} and regularization term \mathcal{L}_{re} jointly.

Retrieval. For each query text \mathbf{x} provided by users or generated by LLMs, we create the corresponding query embedding as $\mathbf{q}_x = \mathbf{W}^q \text{LM}(\mathbf{x}) + \mathbf{b}^q$. Then, we use the k-nearest searching approach to retrieve a set of related papers based on the similarity between the query embedding and the candidate embedding, which is accompanied by the corresponding pseudo-query embedding. The retrieval for query text \mathbf{x} is defined as:

$$V_k(\mathbf{x}) = \arg \top_k \cos(\mathbf{q}_x, \mathbf{c}_n + \mathbf{p}_n), \quad (4)$$

where the $\arg \top_k$ operation retrieves the top- k elements based on the similarity. k is a hyper-parameter, indicating the number of retrieved papers. Our graph retriever, with its neighbor-aware candidate embedding and structure-aware training, effectively captures structural dependencies that previous methods typically overlook. Additionally, by utilizing pseudo-query embedding, our approach can handle sparse contexts and less informative queries, addressing challenges that previous methods struggle with.

Instructions for Citation Graph Understanding

We leverage an LLM as the foundation to unify multiple literature-related tasks. To enhance its capabilities on citation graphs and align it with specialized domain knowledge,

we conduct instruction fine-tuning with LoRA (Hu et al. 2021), using a curated collection of general tasks on citation graphs. This multi-task instruction tuning approach enables the model to learn task-specific behaviors while preserving its general language understanding capabilities.

As illustrated in Figure 2 (C), we design node-level tasks such as *Title Generation* and *Abstract Completion* based on given paper abstracts. These tasks aim to infuse domain-specific context into the LLM backbone and enhance its scientific writing capabilities. By learning to generate titles and complete abstracts, the model develops a deeper understanding of scientific literature and content representation.

We also incorporate edge-level tasks, including *Paper Recommendation*, *Citation Link Prediction*, and *Citation Sentence Generation*. These tasks improve the model’s comprehension of both scientific context and local structures of citation relations. Specifically, *Paper Recommendation* and *Citation Link Prediction* enable the model to understand the relevance and connections between different papers, while *Citation Sentence Generation* helps it learn how citations are integrated into scientific writing, leading to emergent capabilities in handling more complex literature-related queries, such as related work generation.

By combining node-level and edge-level tasks, our approach ensures that the model develops a robust understanding of both the content of individual papers and the relations between them. These tasks collectively form a necessary and sufficient set for the model to develop a comprehensive and foundational understanding of citation relations. Detailed instruction formats for each task are provided in Appendix A.

Inference Pipeline

As shown in Figure 2 (D), LitFM can uniformly handle various literature-related tasks, even for unseen papers, with the knowledge-infused LLM and the graph retriever. The process begins by retrieving relevant papers from the citation graph, which are then used as references. The LLM then extracts the main arguments from these references and infers relations between them. For example, when determining if paper A would cite paper B, LitFM first retrieves potential citations using the graph retriever. The titles and abstracts of two papers, and the retrieved references are fed into the knowledge-infused LLM with task-specific instructions. If the arguments of A and B are relevant or they share similar relations with the references, the response will be “YES”.

Chain-of-Thought Strategy. To demonstrate LitFM’s zero-shot capabilities on the complex tasks, we focus on related work generation, which requires sophisticated synthesis and contextualization of research. Current approaches have several limitations, as they rely on provided context (e.g., ground-truth relationships between papers) or require manual intervention (e.g., manually selecting cited papers). Based on the retriever-augmented pipeline, we introduce a chain-of-thought strategy to handle this task step-by-step, as follows. We refer to Appendix A for more details.

- **Summarize the query text.** The knowledge-infused LLM first summarizes the main arguments of the new paper from the user-provided description, which may con-

tain irrelevant words and sentences.

- **Retrieve related papers.** The summarized text is fed into the graph retriever to retrieve potential cited papers.
- **Recommend cited papers.** To refine the retrieval, we ask the knowledge-infused LLM to recommend the top-k papers most likely to be cited from the retrieved list.
- **Generate citation sentences.** We ask the LLM to generate the citation sentences that describe the relationship between the target paper and each cited paper, which are essential for a comprehensive literature review.
- **Group citation sentences.** The cited papers may include several topics. We ask the LLM to group these citation sentences based on their topics and relevance to the target paper, allowing similar papers to be discussed together.
- **Organize as a related work section.** Finally, we ask the LLM to organize each group of citation sentences into coherent paragraphs and then combine these paragraphs as the related work section of the target paper.

Complexity Analysis. Compared with vanilla LLMs, the additional time complexity of LitFM stems from the graph retriever. First, to generate the neighbor-aware candidate embeddings, we perform message passing, which has a complexity of $O(|\mathcal{N}(i)|d)$, where $|\mathcal{N}(i)|$ indicates the number of neighbor nodes for any node $i \in \mathcal{G}$. Then, during inference, the graph retriever encodes the prompt x using a BERT model, which has a time complexity of $O(|x|^2d)$, where d is the embedding dimension and $|\cdot|$ indicates the token length. Finally, the similarity calculation has a time complexity of $O(d_1)$, where d_1 represents the hidden dimension.

Experiments

Dataset

To establish our framework, we curated three new citation graph benchmark datasets from three distinct domains: medicine, computer science, and physics. Compared with existing citation graph datasets such as ogbn-arxiv-TA (Yan et al. 2023) and Semantic Scholar Network dataset (An et al. 2021), our datasets offer several advantages:

- In addition to each paper’s title and abstract, node attributes in our graph include the paper’s related work section (when available).
- Each edge is annotated with the citing sentence extracted from the citing paper, along with its local context (*i.e.*, the preceding and following sentences), thus capturing how the papers discuss one another. Additionally, each edge contains an indicator variable specifying whether the cited paper is mentioned in the related work section of the citing paper, thus distinguishing between literature review citations and in-paper technical citations.

Our dataset not only facilitates the construction of the dataset for instruction tuning but also allows for the evaluation of downstream tasks detailed in the previous sections and serves as a test bed for assessing the performance of the related work generation task. The medicine portion is constructed based on the PubMed Central repository. Meanwhile, the computer science and physics categories are derived from the LaTeX sources from the arXiv repository. For

dataset statistics, examples, and more detailed information about the construction process, please refer to Appendix B.

Evaluation on Literature-related Tasks

Baselines. For generation tasks, we use four open-source large language models: Mistral 7B (Jiang et al. 2023), Vicuna 7B/13B (Chiang et al. 2023), Llama-3 8B (Touvron et al. 2023), and two closed-source large language models GPT-3.5-turbo and the most recent GPT-4o as baselines. We also employ a typical GNN-based model, GAT (Veličković et al. 2018), as the baseline for citation link prediction and recommendation tasks. To integrate text information, we initialize the node embedding with the BERT-encoded embeddings of the paper title and abstract. The edge embeddings are initialized by the text of citation sentences.

Experimental Settings. For each citation graph, we randomly sample a connected dense sub-graph with 2,000 nodes as the test set. The remaining nodes and edges, excluding those in the test set, constitute the training data used for training the graph retriever and fine-tuning the large language models via the LoRA technique (Hu et al. 2021). We use Vicuna model as the LLM backbone of LitFM. We use the BERT-base-uncased model to yield text embeddings for GNN and graph retriever. For the citation link prediction task, the ratio of positive to negative samples is set to 1 : 1. For the citation recommendation task, the size of the candidate set is fixed at 10 for each query with both negative samples and candidate samples randomly sampled. For the abstract completion task, the first 10% of each abstract is provided as input to the LLM. The number of retrieved papers that are used for augmentations is set as $k \in \{1, 3, 5, 10\}$. We run all the models five times with different random seeds and report the average performance to eliminate deviations. All the experiments are conducted on NVIDIA A40 with 48 GB memory. More details can be found in Appendix C.

Evaluation Metrics. We use Accuracy for the citation link prediction task and Hits@ k for the citation recommendation task. For generation tasks, we follow the previous setting (Zhang et al. 2019) and use the BERTScore to evaluate the semantic similarity of the generated text and the ground truth one. We also measure the relevance of the generated related work using ROUGE-L score (Lin 2004) that calculates the overlap of n-grams between the text of cited papers and the generated related work. We also report the statistics, such as text length and number of citations, in the ground-truth related work and the generated text.

Performance Comparison. As shown in Table 1 and 2, LitFM consistently outperforms other baselines on five evaluation tasks across the three datasets, especially for tasks requiring graph comprehension. On the medicine dataset, LitFM achieves 8.0% improvement in accuracy for citation link prediction and 5.9% in Hits@1 for citation recommendation task, highlighting the effectiveness of our proposed model in reducing hallucinations and filtering out irrelevant information. Additionally, LitFM achieves the best performance on the citation sentence generation task across all three datasets, showing its superiority in reasoning relationships between literature. Notably, LitFM-7B version outper-

Table 1: Performance on the citation link prediction task and the citation recommendation task. We report accuracy for the link prediction and the Hits@1 metric for the recommendation task. The best and the second-best results are shown in **bold** and underlined respectively.

Datasets	Citation Link Prediction			Citation Recommendation		
	CS	Physics	Medicine	CS	Physics	Medicine
GAT + BERT	0.865	0.871	0.882	0.837	0.866	0.857
Vicuna-7b	0.522	0.503	0.519	0.595	0.614	0.451
Vicuna-13b	0.551	0.505	0.557	0.475	0.567	0.504
Mistral-7b	0.578	0.517	0.561	0.625	0.638	0.552
Llama3-8b	0.615	0.522	0.559	0.683	0.682	0.617
GPT 3.5 turbo	0.689	0.617	0.641	0.793	0.845	0.736
GPT 4o	0.728	0.711	0.803	<u>0.883</u>	0.897	0.862
LitFM-7b	0.889	0.895	0.896	0.872	0.901	0.885
LitFM-13b	0.903	0.919	0.953	0.906	0.915	0.908
Improve	4.3%	5.5%	8.0%	8.2%	5.6%	5.9%

Table 2: Performance of existing LLMs and LitFM on generation tasks with Precision and F-score of the BERT score.

Models	Datasets	Title Generation		Abstract Completion		Citation Sentence Generation	
		Precision	F-score	Precision	F-score	Precision	F-score
Vicuna-7b	CS	0.875	0.887	0.873	0.852	0.782	0.796
	Physics	0.866	0.867	<u>0.883</u>	0.854	0.829	0.805
	Medicine	0.870	0.875	0.877	0.848	0.845	0.832
Vicuna-13b	CS	0.875	0.888	0.882	0.854	0.792	0.809
	Physics	<u>0.866</u>	0.868	0.882	0.853	0.829	0.801
	Medicine	0.872	0.877	0.880	0.854	0.834	0.825
Mistral-7b	CS	0.869	0.872	0.872	0.850	0.825	0.809
	Physics	0.827	0.854	0.875	0.861	0.819	0.798
	Medicine	0.859	0.855	0.872	0.840	0.857	0.833
Llama3-8b	CS	0.841	0.866	0.867	0.838	0.821	0.831
	Physics	0.832	0.855	0.846	0.851	0.820	0.799
	Medicine	0.868	0.879	0.879	0.849	0.833	0.827
GPT-3.5 turbo	CS	0.869	0.885	0.877	0.854	0.829	0.816
	Physics	0.862	0.873	0.878	0.855	0.826	0.801
	Medicine	0.862	0.873	0.877	0.849	0.823	0.825
GPT-4o	CS	0.875	0.889	0.857	0.851	0.832	0.824
	Physics	0.864	0.875	0.864	0.853	0.834	0.808
	Medicine	0.889	<u>0.884</u>	0.879	<u>0.854</u>	<u>0.860</u>	0.831
LitFM-7b	CS	0.871	0.880	0.864	<u>0.860</u>	<u>0.836</u>	<u>0.838</u>
	Physics	0.863	0.871	0.875	0.855	0.829	<u>0.818</u>
	Medicine	0.877	0.881	0.887	0.851	0.849	<u>0.836</u>
LitFM-13b	CS	0.880	0.889	<u>0.873</u>	0.863	0.849	0.841
	Physics	0.872	0.878	0.891	0.870	0.837	0.824
	Medicine	<u>0.885</u>	0.890	0.892	0.859	0.863	0.849

forms LLMs with larger parameter sizes, such as Llama3-8b and Vicuna-13b. Interestingly, LitFM shows a more significant improvement on the medicine dataset, which can be attributed to 1) the corpus in this dataset containing many medical terms, thus requiring more domain-specific knowledge, and 2) the sparsity of the medicine test dataset, which benefits more from the neighbor-aware modeling and pseudo-query embedding of the graph retriever model.

Ablation and Analysis. As illustrated in Figure 3 (a), our instruction tuning strategy and the graph-augmented pipeline can be seamlessly adapted to other LLMs to enhance their performance on citation graph tasks, which shows the generalization ability of our proposed strategies. In Figure 3 (b), we observe that the graph retriever enhances performance across most tasks, especially those requiring graph comprehension. For title generation and abstract completion tasks, which require an understanding of the semantics within the paper, the integration of additional information from other papers does not lead to performance degradation, showing the robustness of LitFM in capturing relevant information.

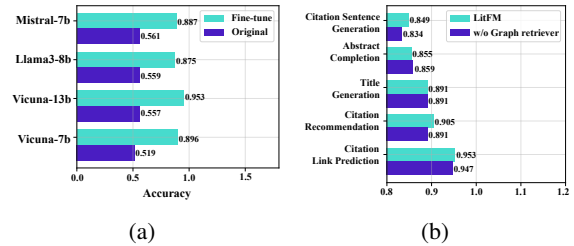


Figure 3: (a) Link prediction performance of existing LLMs with and without knowledge-infused fine-tuning. (b) Performance of LitFM with and without graph retriever.

Table 3: Retrieval performance of different approaches. P@5 and P@10 refer to Precision@5 and Precision@10.

Datasets	CS		Physics		Medicine	
	P@5	P@10	P@5	P@10	P@5	P@10
Models						
G-Retriever (He et al. 2024)	0.286	0.301	0.202	0.305	0.389	0.433
GRAG (Hu et al. 2024)	0.309	0.343	0.208	0.326	0.403	0.467
Graph retriever	0.623	0.760	0.736	0.832	0.723	0.714
w/o pseudo-query embedding	0.519	0.587	0.597	0.643	0.644	0.542
w/o neighbor-aware candidate embedding	0.331	0.357	0.220	0.141	0.351	0.379

Graph Retriever Analysis

Retrieval Accuracy. To analyze the effectiveness of our proposed graph retriever, we compare its retrieval precision with typical graph-aware RAG approaches including G-Retriever (He et al. 2024) and GRAG (Hu et al. 2024), and two variants of our graph retriever: 1) without pseudo-query embedding, and 2) without neighbor-aware candidate embedding. As shown in Table 3, the graph retriever achieves higher retrieval precision compared with existing methods, especially for the sparse physics dataset, showing the effectiveness of the proposed pseudo-query embedding and neighbor-aware candidate embedding in handling sparse context scenarios. Notably, even without pseudo-query embedding, LitFM still consistently outperforms baselines, highlighting the efficacy of neighbor-aware training in capturing the structural context of papers.

Augmentation Effectiveness. Figure 4 (a) shows the performance of LitFM with different retrieving approaches. We observe that LitFM achieves higher generation quality with our graph retriever, especially for the citation link prediction task where inaccurate retrieval can introduce noise text and thus damage the performance. This shows the effectiveness of the graph retriever in accurately enriching citation context. One interesting observation is that using references retrieved by our graph retriever leads to higher accuracy on link prediction task than using the ground-truth references. This can be attributed to the graph retriever’s ability to filter out some papers that are not directly related. Figure 4 (b) illustrates the performance trend as the number of augmentation papers increases. While a larger number of augmentation papers enhances the quality of generated citation sentences, it leads to a slight decline in citation recommendation performance due to the noise introduced by irrelevant papers. Figure 5 demonstrates that LitFM consistently outperforms the retrieval-augmented Vicuna and GPT-3.5 turbo. Notably, Vicuna exhibits performance degradation

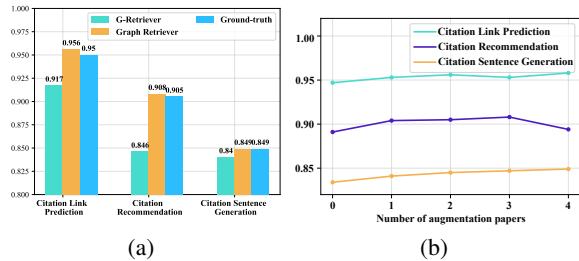


Figure 4: (a) Performance of LitFM when using different retrieving approaches. (b) The performance of LitFM with different number of augmentation papers.

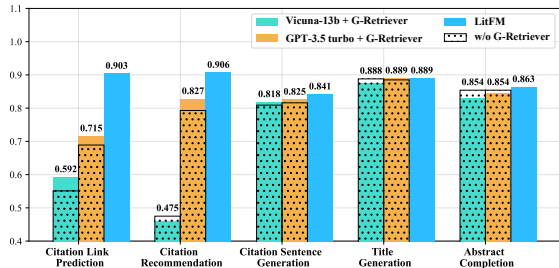


Figure 5: Performance of existing LLMs with G-Retriever on citation graph tasks.

on recommendation and title generation with G-Retriever. This could be attributed to Vicuna’s lack of domain-specific knowledge, which hinders its ability to accurately extract valuable information from augmentation literature.

Related Work Generation Performance

Table 4: Performance of existing LLMs and LitFM on related work generation tasks. We report the F-score of the BERT score and the ROUGE score.

Datasets	CS		Physics	
	BERT Score	ROUGE	BERT Score	ROUGE
Llama3-8b	0.765	0.158	0.671	0.168
Vicuna-13b	0.735	0.191	0.632	0.162
GPT-3.5 turbo	0.801	0.190	0.684	0.170
GPT-4o	<u>0.806</u>	<u>0.221</u>	<u>0.697</u>	<u>0.217</u>
LitFM-13b	0.819 ($\uparrow 1.6\%$)	0.224 ($\uparrow 1.3\%$)	0.766 ($\uparrow 9.8\%$)	0.177

Performance Comparison. As shown in Table 4, LitFM outperforms existing powerful LLMs on related work generation on both BERT and ROUGE score. This demonstrates that the related work section produced by LitFM is more semantically similar to the ground truth and covers more information from the cited papers. Table 5 shows that the statistical distributions of LitFM’s generated content are more aligned with the ground truth, especially for the sparse physics dataset, highlighting the superior generalization ability of LitFM. Although GPT-4o generates longer related work sections, it often fails to segment paragraphs effectively. In contrast, LitFM, benefiting from its knowledge-infused LLM, can better understand literature semantics and achieve more rational segmentation. Moreover, although the related work generated by existing LLMs includes some ci-

Table 5: Statistics Comparison between the generated related work and the ground truth one on the average length (L), average number of paragraphs (NP), average number of citations (NC), and average ratio of paragraphs with citations (RPC). The statistics that are closest to the ground truth are shown in **bold** and the secondary are underlined.

Datasets	CS				Physics			
	L	NP	NC	RPC	L	NP	NC	RPC
Ground Truth	1014.08	7.36	21.44	0.859	701.43	6.44	16.84	0.689
Llama3-8b	<u>378.01</u>	12.15	<u>9.53</u>	<u>0.915</u>	452.90	16.02	8.87	0.874
Vicuna-13b	214.84	3.69	3.77	0.918	249.64	<u>3.67</u>	6.53	0.951
GPT-3.5 turbo	307.05	6.65	4.73	0.736	202.38	2.63	5.36	0.822
GPT-4o	701.11	13.98	9.20	0.781	<u>503.97</u>	11.59	<u>10.04</u>	0.706
LitFM-13b	338.90	<u>5.95</u>	9.57	0.802	504.81	5.81	10.53	<u>0.821</u>

tations, these cited papers may not correspond to real papers. Instead, LitFM generates related work by referring to actual citation graphs, thus reducing the citation hallucinations.

Ablation study. Table 6 examines the effectiveness of each component of LitFM in related work generation. The results show COT improves generation quality by breaking down the complex related work generation task into several simple tasks, such as citation recommendation and citation sentence generation. This step-by-step strategy helps LitFM to accurately extract useful information from the citation graphs. The table also reveals that performance degrades significantly without the graph retriever, especially on the ROUGE score. This decline occurs because, without the augmentation of retrieved papers, the generation often contains many fake citations due to LLM hallucinations. G-Retriever, which fails to consider structural relevance among papers, tends to introduce noise information in downstream tasks. Instead, our graph retriever enhances generation quality by effectively utilizing the structural context of papers.

Table 6: Related work generation performance of different variants. COT refers to the chain-of-thought strategy and RAG refers to graph retriever augmented generation.

Datasets	CS		Physics	
	BERT Score	ROUGE	BERT Score	ROUGE
w/o COT	0.803	0.204	0.621	0.104
w/o Graph retriever	0.792	0.127	0.616	0.096
with G-Retriever	0.798	0.176	0.631	0.164
LitFM-13b	0.819	0.224	0.766	0.177

Case Study. In Appendix D, we conduct case study of LitFM and powerful LLMs (*e.g.*, GPT-3.5 turbo) on the citation sentence generation, title generation, abstract completion, and related work generation tasks.

Conclusion

In this paper, we develop the first literature foundation model LitFM that uniformly handle various citation graph-related tasks. It consists of a graph retriever and a knowledge-infused LLM to avoid hallucinations and generalize to handle new papers outside the citation graph. Extensive experimental results demonstrate both the versatility of LitFM and its superior performance across six benchmark tasks.

References

- Ali, Z.; Kefalas, P.; Muhammad, K.; Ali, B.; and Imran, M. 2020. Deep learning in citation recommendation models survey. *Expert Systems with Applications*, 162: 113790.
- An, C.; Zhong, M.; Chen, Y.; Wang, D.; Qiu, X.; and Huang, X. 2021. Enhancing scientific papers summarization with citation graph. In *Proceedings of the AAAI conference on artificial intelligence*, volume 35, 12498–12506.
- Baek, J.; Jauhar, S. K.; Cucerzan, S.; and Hwang, S. J. 2024. Researchagent: Iterative research idea generation over scientific literature with large language models. *arXiv preprint arXiv:2404.07738*.
- Beltagy, I.; Lo, K.; and Cohan, A. 2019. SciBERT: A pre-trained language model for scientific text. *arXiv preprint arXiv:1903.10676*.
- Chai, Z.; Zhang, T.; Wu, L.; Han, K.; Hu, X.; Huang, X.; and Yang, Y. 2023. Graphllm: Boosting graph reasoning ability of large language model. *arXiv preprint arXiv:2310.05845*.
- Chen, R.; Zhao, T.; Jaiswal, A.; Shah, N.; and Wang, Z. 2024a. Llaga: Large language and graph assistant. *arXiv preprint arXiv:2402.08170*.
- Chen, X.; He, N.; Hu, Y.; and Ye, Z. 2024b. Efficient Algorithms for A Class of Stochastic Hidden Convex Optimization and Its Applications in Network Revenue Management. *arXiv:2205.01774*.
- Chen, Z.; Mao, H.; Wen, H.; Han, H.; Jin, W.; Zhang, H.; Liu, H.; and Tang, J. 2023. Label-free node classification on graphs with large language models (llms). *arXiv preprint arXiv:2310.04668*.
- Chiang, W.-L.; Li, Z.; Lin, Z.; Sheng, Y.; Wu, Z.; Zhang, H.; Zheng, L.; Zhuang, S.; Zhuang, Y.; Gonzalez, J. E.; Stoica, I.; and Xing, E. P. 2023. Vicuna: An Open-Source Chatbot Impressing GPT-4 with 90%* ChatGPT Quality.
- Devlin, J.; Chang, M.-W.; Lee, K.; and Toutanova, K. 2019. BERT: Pre-training of Deep Bidirectional Transformers for Language Understanding. In *Proceedings of the 2019 Conference of the North American Chapter of the Association for Computational Linguistics: Human Language Technologies, Volume 1 (Long and Short Papers)*, 4171–4186.
- Fatemi, B.; Halcrow, J.; and Perozzi, B. 2023. Talk like a graph: Encoding graphs for large language models. *arXiv preprint arXiv:2310.04560*.
- Gao, Y.; Xiong, Y.; Gao, X.; Jia, K.; Pan, J.; Bi, Y.; Dai, Y.; Sun, J.; and Wang, H. 2023. Retrieval-augmented generation for large language models: A survey. *arXiv preprint arXiv:2312.10997*.
- Gilmer, J.; Schoenholz, S. S.; Riley, P. F.; Vinyals, O.; and Dahl, G. E. 2017. Neural message passing for quantum chemistry. In *International conference on machine learning*, 1263–1272. PMLR.
- Gu, Y.; Tinn, R.; Cheng, H.; Lucas, M.; Usuyama, N.; Liu, X.; Naumann, T.; Gao, J.; and Poon, H. 2021. Domain-specific language model pretraining for biomedical natural language processing. *ACM Transactions on Computing for Healthcare (HEALTH)*, 3(1): 1–23.
- Hamilton, W.; Ying, Z.; and Leskovec, J. 2017. Inductive representation learning on large graphs. *Advances in neural information processing systems*, 30.
- He, X.; Tian, Y.; Sun, Y.; Chawla, N. V.; Laurent, T.; LeCun, Y.; Bresson, X.; and Hooi, B. 2024. G-retriever: Retrieval-augmented generation for textual graph understanding and question answering. *arXiv preprint arXiv:2402.07630*.
- Hu, E. J.; Shen, Y.; Wallis, P.; Allen-Zhu, Z.; Li, Y.; Wang, S.; Wang, L.; and Chen, W. 2021. Lora: Low-rank adaptation of large language models. *arXiv preprint arXiv:2106.09685*.
- Hu, Y.; Lei, Z.; Zhang, Z.; Pan, B.; Ling, C.; and Zhao, L. 2024. GRAG: Graph Retrieval-Augmented Generation. *arXiv preprint arXiv:2405.16506*.
- Huang, X.; Han, K.; Bao, D.; Tao, Q.; Zhang, Z.; Yang, Y.; and Zhu, Q. 2023. Prompt-based node feature extractor for few-shot learning on text-attributed graphs. *arXiv preprint arXiv:2309.02848*.
- Huang, X.; Han, K.; Yang, Y.; Bao, D.; Tao, Q.; Chai, Z.; and Zhu, Q. 2024. Can GNN be Good Adapter for LLMs? In *Proceedings of the ACM on Web Conference 2024*, 893–904.
- Iqbal, S.; Hassan, S.-U.; Aljohani, N. R.; Alelyani, S.; Nawaz, R.; and Bornmann, L. 2021. A decade of in-text citation analysis based on natural language processing and machine learning techniques: an overview of empirical studies. *Scientometrics*, 126(8): 6551–6599.
- Jiang, A. Q.; Sablayrolles, A.; Mensch, A.; Bamford, C.; Chaplot, D. S.; Casas, D. d. I.; Bressand, F.; Lengyel, G.; Lample, G.; Saulnier, L.; et al. 2023. Mistral 7B. *arXiv preprint arXiv:2310.06825*.
- Jiang, X.; Zhang, R.; Xu, Y.; Qiu, R.; Fang, Y.; Wang, Z.; Tang, J.; Ding, H.; Chu, X.; Zhao, J.; et al. 2024. HyKGE: A Hypothesis Knowledge Graph Enhanced Framework for Accurate and Reliable Medical LLMs Responses. *arXiv preprint arXiv:2312.15883*.
- Jie, Y. W.; Satapathy, R.; Mong, G. S.; Cambria, E.; et al. 2024. How Interpretable are Reasoning Explanations from Prompting Large Language Models? *arXiv preprint arXiv:2402.11863*.
- Jung, S.-Y.; Lin, T.-H.; Liao, C.-H.; Yuan, S.-M.; and Sun, C.-T. 2023. Intent-controllable citation text generation. *Mathematics*, 10(10): 1763.
- Kang, M.; Kwak, J. M.; Baek, J.; and Hwang, S. J. 2023. Knowledge graph-augmented language models for knowledge-grounded dialogue generation. *arXiv preprint arXiv:2305.18846*.
- Kingma, D. P.; and Ba, J. 2014. Adam: A method for stochastic optimization. *arXiv preprint arXiv:1412.6980*.
- Kunnath, S. N.; Pride, D.; and Knoth, P. 2023. Prompting strategies for citation classification. In *Proceedings of the 32nd ACM International Conference on Information and Knowledge Management*, 1127–1137.
- Lee, J.; Yoon, W.; Kim, S.; Kim, D.; Kim, S.; So, C. H.; and Kang, J. 2020. BioBERT: a pre-trained biomedical language representation model for biomedical text mining. *Bioinformatics*, 36(4): 1234–1240.

- Li, X.; and Ouyang, J. 2024a. Explaining Relationships Among Research Papers. *arXiv preprint arXiv:2402.13426*.
- Li, X.; and Ouyang, J. 2024b. Related Work and Citation Text Generation: A Survey. *arXiv preprint arXiv:2404.11588*.
- Li, Y.; Ding, K.; and Lee, K. 2023. GRENADE: Graph-Centric Language Model for Self-Supervised Representation Learning on Text-Attributed Graphs. *arXiv preprint arXiv:2310.15109*.
- Lin, C.-Y. 2004. Rouge: A package for automatic evaluation of summaries. In *Text summarization branches out*.
- Liu, X.; Zhang, J.; and Guo, C. 2013. Full-text citation analysis: A new method to enhance scholarly networks. *Journal of the American Society for Information Science and Technology*, 64(9): 1852–1863.
- Loshchilov, I.; and Hutter, F. 2017. Decoupled weight decay regularization. *arXiv preprint arXiv:1711.05101*.
- Luo, Z.; Song, X.; Huang, H.; Lian, J.; Zhang, C.; Jiang, J.; Xie, X.; and Jin, H. 2024. GraphInstruct: Empowering Large Language Models with Graph Understanding and Reasoning Capability. *arXiv preprint arXiv:2403.04483*.
- Luo, Z.; Xie, Q.; and Ananiadou, S. 2023. Citationsum: Citation-aware graph contrastive learning for scientific paper summarization. In *Proceedings of the ACM Web Conference 2023*, 1843–1852.
- Luo, Z.; Xu, C.; Zhao, P.; Geng, X.; Tao, C.; Ma, J.; Lin, Q.; and Jiang, D. 2023. Augmented large language models with parametric knowledge guiding. *arXiv preprint arXiv:2305.04757*.
- Martin-Boyle, A.; Tyagi, A.; Hearst, M. A.; and Kang, D. 2024. Shallow Synthesis of Knowledge in GPT-Generated Texts: A Case Study in Automatic Related Work Composition. *arXiv preprint arXiv:2402.12255*.
- Minaee, S.; Mikolov, T.; Nikzad, N.; Chenaghlu, M.; Socher, R.; Amatriain, X.; and Gao, J. 2024. Large language models: A survey. *arXiv preprint arXiv:2402.06196*.
- Oord, A. v. d.; Li, Y.; and Vinyals, O. 2018. Representation learning with contrastive predictive coding. *arXiv preprint arXiv:1807.03748*.
- Ren, X.; Tang, J.; Yin, D.; Chawla, N.; and Huang, C. 2024. A Survey of Large Language Models for Graphs. *arXiv preprint arXiv:2405.08011*.
- Shen, J.; Zhou, T.; Zhao, S.; Chen, Y.; and Liu, K. 2024. Citekit: A Modular Toolkit for Large Language Model Citation Generation. *arXiv preprint arXiv:2408.04662*.
- Shen, W.; Gao, Y.; Huang, C.; Wan, F.; Quan, X.; and Bi, W. 2023. Retrieval-Generation Alignment for End-to-End Task-Oriented Dialogue System. *arXiv preprint arXiv:2310.08877*.
- Sun, L.; Han, Y.; Zhao, Z.; Ma, D.; Shen, Z.; Chen, B.; Chen, L.; and Yu, K. 2024. Scieval: A multi-level large language model evaluation benchmark for scientific research. In *Proceedings of the AAAI Conference on Artificial Intelligence*, volume 38, 19053–19061.
- Tang, J.; Yang, Y.; Wei, W.; Shi, L.; Su, L.; Cheng, S.; Yin, D.; and Huang, C. 2024a. Graphgpt: Graph instruction tuning for large language models. In *Proceedings of the 47th International ACM SIGIR Conference on Research and Development in Information Retrieval*, 491–500.
- Tang, J.; Yang, Y.; Wei, W.; Shi, L.; Xia, L.; Yin, D.; and Huang, C. 2024b. Higt: Heterogeneous graph language model. *arXiv preprint arXiv:2402.16024*.
- Touvron, H.; Lavril, T.; Izacard, G.; Martinet, X.; Lachaux, M.-A.; Lacroix, T.; Rozière, B.; Goyal, N.; Hambro, E.; Azhar, F.; et al. 2023. Llama: Open and efficient foundation language models. *arXiv preprint arXiv:2302.13971*.
- Tsai, H.-J.; Yen, A.-Z.; Huang, H.-H.; and Chen, H.-H. 2023. Citation Intent Classification and Its Supporting Evidence Extraction for Citation Graph Construction. In *Proceedings of the 32nd ACM International Conference on Information and Knowledge Management*, 2472–2481.
- Veličković, P.; Cucurull, G.; Casanova, A.; Romero, A.; Liò, P.; and Bengio, Y. 2018. Graph Attention Networks. In *International Conference on Learning Representations*.
- Wang, X.; Yang, Q.; Qiu, Y.; Liang, J.; He, Q.; Gu, Z.; Xiao, Y.; and Wang, W. 2023. Knowledgpt: Enhancing large language models with retrieval and storage access on knowledge bases. *arXiv preprint arXiv:2308.11761*.
- Wei, J.; Wang, X.; Schuurmans, D.; Bosma, M.; Xia, F.; Chi, E.; Le, Q. V.; Zhou, D.; et al. 2022. Chain-of-thought prompting elicits reasoning in large language models. *Advances in neural information processing systems*, 35: 24824–24837.
- Xia, L.; Kao, B.; and Huang, C. 2024. Opengraph: Towards open graph foundation models. *arXiv preprint arXiv:2403.01121*.
- Yan, H.; Li, C.; Long, R.; Yan, C.; Zhao, J.; Zhuang, W.; Yin, J.; Zhang, P.; Han, W.; Sun, H.; et al. 2023. A comprehensive study on text-attributed graphs: Benchmarking and rethinking. *Advances in Neural Information Processing Systems*, 36: 17238–17264.
- Yang, C.; and Han, J. 2023. Revisiting citation prediction with cluster-aware text-enhanced heterogeneous graph neural networks. In *2023 IEEE 39th International Conference on Data Engineering (ICDE)*, 682–695.
- Zha, L.; Zhou, J.; Li, L.; Wang, R.; Huang, Q.; Yang, S.; Yuan, J.; Su, C.; Li, X.; Su, A.; et al. 2023. Tablegpt: Towards unifying tables, nature language and commands into one gpt. *arXiv preprint arXiv:2307.08674*.
- Zhang, T.; Kishore, V.; Wu, F.; Weinberger, K. Q.; and Artzi, Y. 2019. Bertscore: Evaluating text generation with bert. *arXiv preprint arXiv:1904.09675*.
- Zhang, Y.; Cheng, H.; Shen, Z.; Liu, X.; Wang, Y.-Y.; and Gao, J. 2023a. Pre-training multi-task contrastive learning models for scientific literature understanding. *arXiv preprint arXiv:2305.14232*.
- Zhang, Y.; Li, Y.; Cui, L.; Cai, D.; Liu, L.; Fu, T.; Huang, X.; Zhao, E.; Zhang, Y.; Chen, Y.; et al. 2023b. Siren’s song in the AI ocean: a survey on hallucination in large language models. *arXiv preprint arXiv:2309.01219*.

Zhang, Y.; Wang, Y.; Wang, K.; Sheng, Q. Z.; Yao, L.; Mahmood, A.; Zhang, W. E.; and Zhao, R. 2023c. When Large Language Models Meet Citation: A Survey. *arXiv preprint arXiv:2309.09727*.

Zhang, Z.; Fang, M.; Chen, L.; Namazi-Rad, M.-R.; and Wang, J. 2023d. How do large language models capture the ever-changing world knowledge? a review of recent advances. *arXiv preprint arXiv:2310.07343*.

Zhao, J.; Zhuo, L.; Shen, Y.; Qu, M.; Liu, K.; Bronstein, M.; Zhu, Z.; and Tang, J. 2023. Graphtext: Graph reasoning in text space. *arXiv preprint arXiv:2310.01089*.

Zhao, P.; Zhang, H.; Yu, Q.; Wang, Z.; Geng, Y.; Fu, F.; Yang, L.; Zhang, W.; and Cui, B. 2024. Retrieval-augmented generation for ai-generated content: A survey. *arXiv preprint arXiv:2402.19473*.

Appendix A: Instruction Paradigm

As shown in Figure 6, we provide the detailed instruction prompt for each fine-tuning task. The instruction prompt can be seamlessly instantiated through the domain literature and used to inject domain-specific knowledge into the LLM. As illustrated in Figure 7, we provide detailed chain-of-thought instructions for related work generation.

Appendix B: Dataset Details

Extraction Procedure

Arxiv Papers To create the citation graphs for the CS and physics category, we start with a cleaning procedure that involves the following: 1) removing comments, 2) flattening LaTeX sources, 3) substituting user-defined macros with standard LaTeX commands, 4) eliminating LaTeX native commands, and 5) standardizing citation commands. Next, we identified and parsed the bibliography file (.bib) to create a dictionary mapping citation IDs to arXiv paper IDs. In cases where a .bib file was unavailable, we processed the .bbl file instead. If neither was present, we extracted inline citations using the LaTeX ‘thebibliography’ environment.

After extracting both the content and the citation library, we proceeded to locate citations within each paper. For each citation, we extracted the citing sentence and the local context (defined as the preceding and following sentences). Additionally, we extracted the “Related Work” sections from each paper. A related work section is identified by titles such as “Related Work,” “Literature Review,” “Related Research,” “Existing Research,” and 20 other possible variations we defined to find a match. If no match is found, we use the “Introduction” section as an alternative. Finally, for each citation, we provide an indicator variable that specifies whether the citation belongs to the related work section.

PubMed papers For PubMed Central papers, we begin our cleaning process by filtering out XML files that do not have PMIDs. Next, we unify the citation style, converting superscript numbers and author names to citations within brackets [·]. Using regular expressions, we then extract citations and map them to the PMIDs of the papers in the graph. Similar to our approach with arXiv papers, we extract the citing sentence and local context for each citation. We also extract the related work section using the same procedure, mapping section titles to predefined possible matches, with the introduction taken as the default last resort. Finally, for each citation, we provide an indicator variable specifying whether the citation belongs to the related work section.

Examples

The statistics of our datasets are provided in Table 7. We further provide below an example of a node and an edge in each citation graph category. The [...] symbol is inserted below to reduce the size of the related work.

Node ID: 36234872

Title: Influence of the Epoxy/Acid Stoichiometry on the Cure Behavior and Mechanical Properties of Epoxy

Table 7: Statistics of the citations graphs.

	#Nodes	#Edges	#Related Works
Medicine	2.1M	7.4M	1.5M
Computer Science	340k	3.2M	188k
Physics	59k	120k	19k

Vitrimers

Abstract: Bisphenol A epoxy resin cured with a mixture of dimerized and trimerized fatty acids is the first epoxy vitrimer and has been extensively studied. However, the cure behavior and thermal and mechanical properties of this epoxy vitrimer depend on the epoxy/acid stoichiometry. To address these issues, epoxy vitrimers with three epoxy/acid stoichiometries (9:11, 1:1 and 11:9) were prepared and recycled four times. Differential scanning calorimetry (DSC) was used to study the cure behavior of the original epoxy vitrimers. The dynamic mechanical properties and mechanical performance of the original and recycled epoxy vitrimers were investigated by using dynamic mechanical analysis (DMA) and a universal testing machine. Furthermore, the reaction mechanism of epoxy vitrimer with different epoxy/acid stoichiometry was interpreted. With an increase in the epoxy/acid ratio, the reaction rate, swelling ratio, glass transition temperature and mechanical properties of the original epoxy vitrimers decreased, whereas the gel content increased. The recycling decreased the swelling ratio and elongation at break of the original epoxy vitrimers. Moreover, the elongation at break of the recycled epoxy vitrimers decreased with the epoxy/acid ratio at the same recycling time. However, the gel content, tensile strength and toughness of the original epoxy vitrimers increased after the recycling. The mechanical properties of epoxy vitrimers can be tuned with the variation in the epoxy/acid stoichiometry.

Related Work: 1. Introduction Epoxy resin, one of the most important and popular classes of thermosetting polymers, is firmly rooted in many areas, both in our daily lives and in industry [1,2,3,4,5]. Due to its outstanding mechanical strength, dimensional and thermal stability, as well as creep, chemical and electrical insulation resistance, epoxy resin has been widely used in construction, adhesives, electronic and electrical devices, coatings, composites and so on [1,6,7,8,9,10]. However, due to their insoluble and infusible nature, the irreversible covalent networks restrict epoxy resin from being recycled and reprocessed [...] To investigate the effect of recycling on the solvent stability, thermal and mechanical properties of the original epoxy vitrimers, solvent immersion, dynamic mechanical analysis (DMA) and uniaxial tests were performed.

Edge ID: (‘36234872’, ‘28757995’)

Sentence: To solve these problems, a thrust to develop a novel class of thermosetting polymers with recyclable, healable and reprocessable features has been carried out during the last two decades [11,12].

Preceding Sentence: Thus, most of the epoxy wastes are

Title Generation Prompt	Abstract Completion Prompt	Citation Link Prediction Prompt	Citation Recommendation Prompt	Citation Sentence Generation Prompt
<p>Human: Here is the abstract of paper A, please generate the title of paper A. Abstract: {abstract of paper A}.</p> <p>Graph Augmentation: You can refer to the titles of other papers related to paper A. 1. {title of neighboring paper a}. 2. {title of neighboring paper b}.</p> <p>Response: Title of paper A: {title of paper A}.</p>	<p>Human: Here is the title of paper A, please complete the abstract of paper A. Title: {title of paper A}. Abstract: {partial abstract of paper A}</p> <p>Graph Augmentation: You can refer to the abstracts of other papers related to paper A. 1. {abstract of neighboring paper a}. 2. {abstract of neighboring paper b}.</p> <p>Response: Abstract of paper A: {abstract of paper A}.</p>	<p>Human: Here is the title and abstract of paper A and paper B. Title A: {title of paper A}. Abstract A: {abstract of paper A} Title B: {title of paper B}. Abstract B: {abstract of paper B}</p> <p>Graph Augmentation: Determine if paper A will cite paper B.</p> <p>Graph Augmentation: Other cited paper of paper A: 1. {title of cited paper a}. 2. {title of cited paper b}.</p> <p>Other papers that cite paper B: 1. {title of citing paper c}. 2. {title of citing paper d}.</p> <p>Response: {YES or NO}</p>	<p>Human: Here is the title and abstract of paper A. Title: {title of paper A}. Abstract: {abstract of paper A}</p> <p>Graph Augmentation: Which of the following papers is more likely to be cited by paper A? 1. {title of candidate paper a}. 2. {title of candidate paper b}.</p> <p>Graph Augmentation: Other papers that cite paper a: 1. {title of citing paper m}. 2. {title of citing paper n}.</p> <p>Other papers that cite paper b: 1. {title of citing paper x}. 2. {title of citing paper y}.</p> <p>Response: {Index number of the candidate paper}</p>	<p>Human: Here is the title and abstract of paper A and paper B. Title A: {title of paper A}. Abstract A: {abstract of paper A} Title B: {title of paper B}. Abstract B: {abstract of paper B}</p> <p>Graph Augmentation: Please generate the citation sentence for paper A that cites paper B.</p> <p>Graph Augmentation: Citation sentence of other papers that cite paper B: 1. {sentence between paper a and B}. 2. {sentence between paper b and B}.</p> <p>Response: Citation sentence: {sentence between paper A and B}</p>

Figure 6: Instruction prompt for fine-tuning tasks

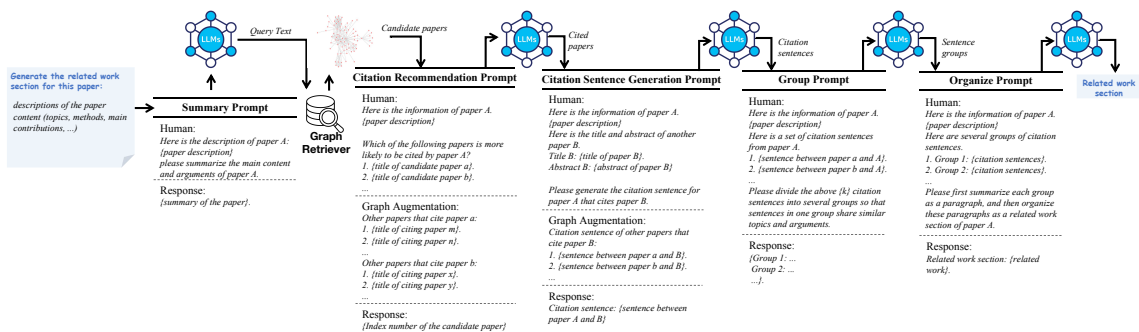


Figure 7: Illustration of the chain-of-chain strategy used for relation work generation.

disposed of by landfill or incineration, which has caused not only a waste of resources but also environmental pollution.

Following Sentence: In 2011, Leibler et al developed a new class of polymers, called vitrimer, based on associative covalent adaptable networks of epoxy resins cured with a mixture of dimerized and trimerized fatty acids through transesterification reactions [13].

In Related Work: True

Category: **Medicine**

Node ID: 2402.07245

Title: Semi-Mamba-UNet: Pixel-Level Contrastive Cross-Supervised Visual Mamba-based UNet for Semi-Supervised Medical Image Segmentation

Abstract: Medical image segmentation is essential in diagnostics, treatment planning, and healthcare, with deep learning offering promising advancements. Notably, Convolutional Neural Network (CNN) excel in capturing local image features, whereas Vision Transformer (ViT) adeptly model long-range dependencies through multi-head self-attention mechanisms. Despite their strengths, both CNN and ViT face challenges in efficiently processing long-range dependencies within medical images, often requiring substantial computational resources. This issue, combined with the high cost and limited availability of expert annotations, poses significant obstacles to achieving precise segmentation. To address these challenges, this

paper introduces the Semi-Mamba-UNet, which integrates a visual mamba-based UNet architecture with a conventional UNet into a semi-supervised learning (SSL) framework. This innovative SSL approach leverages dual networks to jointly generate pseudo labels and cross supervise each other, drawing inspiration from consistency regularization techniques. Furthermore, we introduce a self-supervised pixel-level contrastive learning strategy, employing a projector pair to further enhance feature learning capabilities. Our comprehensive evaluation on a publicly available MRI cardiac segmentation dataset, comparing against various SSL frameworks with different UNet-based segmentation networks, highlights the superior performance of Semi-Mamba-UNet. The source code has been made publicly accessible.

Related Work: Medical image segmentation is essential in enabling precise diagnostics and effective treatment strategies, and deep learning-based networks, particularly those based on the CNN-based UNet architecture, have been extensively investigated [...] The source code of Semi-Mamba-UNet and all baseline methods are made public available.

Edge ID: ('2402.07245', '1804.03999')

Sentence: For example, U-Net++ \cite{zhou2018unet++} introduces a nested UNet structure with deep supervision mechanisms, while Attention UNet \cite{oktay2018attention} incorporates attention gates to bolster the decoders' feature learning capabilities.

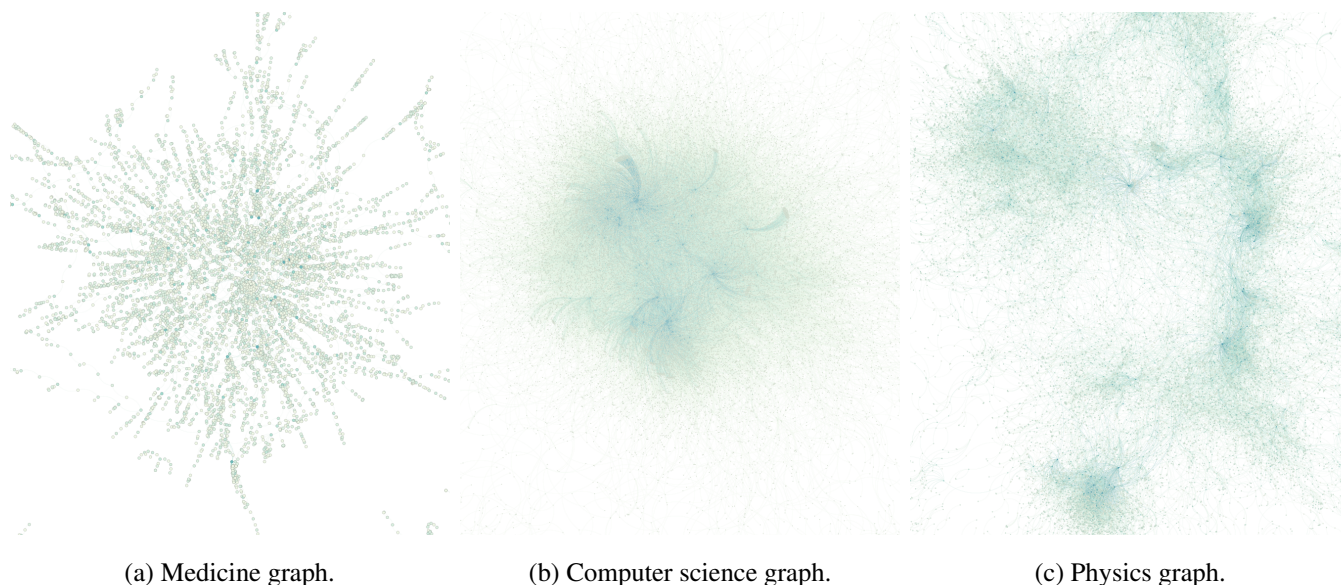


Figure 8: Visualization of the academic graphs.

Preceding Sentence: UNet has catalyzed the development of numerous enhancements.

Following Sentence: Moreover, Res-UNet\cite{diakogiannis2020resunet} integrates residual learning\cite{he2016deep} within its network blocks.

In Related Work: True

Category: [Computer Science](#)

Node ID: 2302.13728

Title: Geometry induced domain-walls of dipole lattices on curved structures

Abstract: We investigate the ground state properties of rectangular dipole lattices on curved surfaces. The curved geometry can ‘distort’ the lattice and lead to dipole equilibrium configurations that strongly depend on the local geometry of the surface. We find that the system’s ground state can exhibit domain-walls separating domains with different dipole configurations. Furthermore, we show how, regardless of the surface geometry, the domain-walls locate along the lattice sites for which the (Euclidean) distances to nearest and next-nearest neighbors are equal. We analyze the response of the domain-walls to an external electric field and observe displacements and splittings thereof below and above a critical electric field, respectively. We further show that the domain-wall acts as a boundary that traps low-energy excitations within a domain.

Related Work: Topology based concepts are widely used for the description of physical systems. A prominent example is that of domains and domain-walls (DW) arising from spontaneous symmetry breaking [.....]. Finally, our results are summarized in Sec. \ref{Sec:Summary}.

Edge ID: (‘2302.13728’, ‘1510.04481’)

Sentence: These studies range from experimental investigations (eg of the dipole equilibrium configurations in stacks of BTA (trialkylbenzene-1,3,5-tricarboxamide) molecules \cite{cornelissen2019,urbanaviciute2019})

to model systems, such as Hubbard models with long-range hopping terms \cite{xiong1992,wang1991,stockhofe2015a,stockhofe2016,guo2020}.

Preceding Sentence: The first steps in this direction were already done in studies of dipoles confined to cylindrical or helical geometries.

Following Sentence: Already in such (comparatively) simple curved geometries, the GS properties show a strong dependence on the geometrical parameters: for example, for dipoles with fixed positions along a helical path, it was demonstrated that the GS configurations are described by a complex self-similar bifurcation diagram \cite{siemens2022}.

In Related Work: True

Category: [Physics](#)

Visualizations

In this subsection, we provide visualizations of each academic graph. These visualizations highlight the graph density, the concentration of citations in specific fields, and the overall connectivity of the graphs. The visualization is performed using Yifan Hu’s (Chen et al. 2024b) algorithm by taking a random connected subgraph of 30k nodes, with nodes in darker colors representing those with high in-degree (i.e., citation counts), as seen in Fig. 8. As seen in the visualizations, the CS graph is the densest, mainly due to the surge of papers, most of which are available on arXiv. For physics, the graph is less dense because it focuses on a subcategory of general physics, and inter-domain physics papers are not captured. As for the medicine graph, the sparsity is due to the small number of nodes compared to the full graph. However, there is still a medium level of connectivity between the papers, with a concentration of citations among a small number of papers.

Appendix C: Implementation Details

Fine-tune LLM. We construct LitFM-7b and LitFM-13b by fine-tuning vicuna-7b and vicuna-13b on domain-specific literature through our proposed institution paradigm. During fine-tuning, the LLMs are loaded in 8-bits and the rank of LoRa is set as 8. Only the **Q**, **K**, **V**, and **O** matrices within a large language model will be updated during fine-tuning. We set the batch size to 2 with the maximum number of update steps to 40000, and the gradient accumulation step to 8. The learning rate is set as 0.0002 and we use AdamW (Loshchilov and Hutter 2017) for optimization. The scaling hyperparameter *lora.alpha* is set to 32, and the dropout rate during fine-tuning is set to 0.05. To construct the training instruction set for each citation graph dataset, we randomly sample 20,000 nodes from the citation graph and use the title and abstract part of each paper to construct the title generation instructions and the abstract completion instructions. We extract the induced subgraph of these nodes to construct other instructions. Specifically, each edge in the induced subgraph will be used to construct a positive citation link prediction instruction. Then, we replace the target node of the edge with a random node to construct a negative citation link prediction instruction. The ratio of positive to negative samples is set to 1:1. Each citation sentence generation instruction is constructed based on the citation sentence of each edge as well as the titles and abstracts of the connected nodes. For citation recommendation instructions, we randomly sample 10 negative nodes for each edge to construct the candidate set. These instructions will be gathered and shuffled during fine-tuning.

Graph retriever. We train the graph retriever model with Adam (Kingma and Ba 2014) optimizer. The number of training epochs is set as 500 and we use the early stopping strategy with a patience of 5. To integrate the text information, we use the pre-trained language model (i.e., BERT-base-uncased³) to get the representations of text attributes, and then these representations are used to initialize the embeddings of nodes and edges in models. The dimensions of the pre-trained representations are 768 and the maximum text length is set as 512. The BERT model is frozen during training. We set the number of negative samples and the maximum number of neighbor nodes as 10. We use random sampling to generate negative samples. We randomly split the edges in citation graphs into train/validation/test sets by 7:1.5:1.5 and select the best model based on the Precision@5 metric on the validation set.

Baselines. During inference, the baseline LLMs (e.g., vicuna 7b/13b and GPT) share the same instruction form as our LitFM. For all of them, we set the temperature as 0.7 and the nucleus sampling size (i.e., *top.p*) is set as 0.95, these two hyperparameters are used to control the randomness of LLMs’ output. The repetition penalty is set as 1.15 to discourage the repetitive and redundant output. The maximum number of tokens that the LLM generates is set as 1024. We ran all the models five times with different random seeds and reported the average performance to eliminate deviations.

³<https://huggingface.co/google-bert/bert-base-uncased>

Appendix D: Case Study

Title and abstract generation. As shown in Figure 9, the red-colored text indicates the content that exists in the ground-truth title, and the green-colored text indicates the content that has not been included in the ground-truth title and abstract, which demonstrates the hallucinations of LLM. We can see that the title generated by LitFM is more similar to the ground-truth title without fake information, showcasing the effectiveness of our knowledge-infused LLM in avoiding Knowledge hallucinations. Moreover, LitFM gets more brief titles than vicuna-13b and GPT-3.5 turbo, which may be because of the better summary ability of LitFM. Especially, in the second example, we can see that vicuna-13b suffers from the logical error. It wrongly describes the relationship between “Sensing and Communication” and “Multi-Domain Cooperation”. Instead, LitFM can accurately infer relationships between different concepts.

In Figure 10, we can see that the generated abstract of LitFM can include the most concepts and keywords existing in the ground-truth abstract section. Because only limited information (i.e., the paper’s title) is provided for the LLM to generate the abstract, all of these models inevitably contain hallucinations. However, compared with vicuna-13b and GPT-3.5 turbo, LitFM can more accurately predict the potential techniques and knowledge because of the Knowledge-infused LLM.

Citation sentence generation. In Figure 11, we provide the generation examples of different LLMs on the citation sentence generation task. There are two main observations: 1) Thanks to the Knowledge-infused LLM, LitFM can extract the main arguments of the paper and thus more accurately describe the previous work in the citation sentence. For example, LitFM accurately extracts the keyword “high resolution” from the cited paper. Instead, the generated sentences of vicuna-13b and GPT-3.5 turbo contain fake information such as “we extend these ideas to demonstrate ...”. 2) Thanks to the graph retriever, LitFM can refer to the citation sentences of other papers and thus more accurately describe the relationship between papers. For example, in the second generation example, LitFM can accurately describe their relationships as “Following” rather than “In contrast to” and “Building on” generated by vicuna-13b and GPT-3.5 turbo.

Related work generation. As illustrated in Figure 12, LitFM has several advantages in generating literature reviews compared with existing powerful LLM such as GPT-3.5 turbo. Firstly, It contains more domain-specific words such as “OLink proteomics”, “scRNA-Seq”, and “zero-forcing beamforming”, showing that LitFM contains more domain-specific knowledge. Moreover, LitFM can generate related work sections with explicit citations, and all cited papers are extracted from the citation graph. However, the generation of GPT 3.5-turbo contains fake citations. Finally, LitFM shows more reasonable paragraph segmentation compared with GPT 3.5-turbo. This is because our COT strategy has explicitly asked the LitFM to group different papers based on their topic and thus achieves a better summary of these cited papers.

Abstract	Ground-truth	Vicuna-13b	GPT-3.5 turbo	LitFM-13b
<p>We theoretically study the dynamics and spatio-temporal pattern formation of driven lattices of nonlinear optical microresonators and analyze the formation of dissipative structures, in particular dissipative Kerr solitons. We consider both equally coupled one-dimensional chains, as well as the topological Su-Schrieffer-Heeger model. We show the complexity of the four-wave mixing pathways arising in these systems with the increasing dimensionality due to the combined spatial and synthetic frequency dimension of each resonator, and show that it can be modeled using a two-dimensional variant of the Lugiato-Lefever equation. We demonstrate the existence of two fundamentally different dynamical regimes in one-dimensional chains - elliptic and hyperbolic - inherent to the system. In the elliptic regime, we generate hexagonal patterns and a two-dimensional dissipative Kerr soliton corresponding to the global spatio-temporal mode-locking and discuss its similarity to edge-state solitons in the two-dimensional Haldane topological lattice. We find that the presence of the second dimension leads to the observation of regularized wave collapse. Furthermore, we study similarities and differences between a one-dimensional topological lattice and a single cavity and analyze nonlinearly induced edge-to-bulk scattering in the Su-Schrieffer-Heeger model. Moreover, we show that soliton formation can both be impaired in trivial but, importantly, also topologically protected bands due to nonlinear bulk edge scattering.</p>	<p>Dissipative structures in topological lattices of nonlinear optical resonators</p>	<p>Dynamics and Spatio-Temporal Pattern Formation of Driven Nonlinear Optical Microresonators</p>	<p>Spatio-Temporal Dynamics and Dissipative Kerr Soliton Formation in Nonlinear Optical Microresonator Lattices: A Study of Topological and Non-Topological Systems</p>	<p>Dissipative solitons in one- and two-dimensional topological lattices of nonlinear optical resonators</p>
<p>With the continuous increase of the spectrum and antennas, endogenous sensing is now possible in the fifth generation and future wireless communication systems. However, sensing is a highly complex task for a heterogeneous communication network with massive connections. Seeking multi-domain cooperation is necessary. In this article, we present an integrated sensing and communication (ISAC) system that performs active, passive, and interactive sensing in different stages of communication through hardware and software. We also propose different methods about how multi-user and multi-frequency band cooperate to further enhance the ISAC system's performance. Finally, we elaborate on the advantages of multi-domain cooperation from the physical layer to the network layer for the ISAC system.</p>	<p>Integrated Sensing and Communication with Multi-Domain Cooperation</p>	<p>Integrated Sensing and Communication System for Multi-Domain Cooperation in Future Wireless Networks</p>	<p>Enhancing Integrated Sensing and Communication (ISAC) Systems: Multi-Domain Cooperation and Performance Optimization in Future Wireless Networks</p>	<p>Integrated Sensing and Communication System: Multi-Domain Cooperation</p>
<p>We analytically show how a superposition of beamlets produces terahertz radiation with greater spatial homogeneity and efficiency compared to tilted-pulse-fronts generated by diffraction gratings. The advantages are particularly notable for large pump bandwidths and beam sizes, alluding to better performance in the presence of cascading effects and higher energy pumping. A theory of terahertz generation using a superposition of beamlets is developed. It is shown how such an arrangement produces a distortion free tilted-pulse-front. Closed form expressions for terahertz spectra and transients in three spatial dimensions are derived. Conditions for obtaining performance parity and bounds for optimal parameters are furnished.</p>	<p>Terahertz generation by beamlet superposition</p>	<p>Superposition of Beamlets for Efficient Terahertz Radiation</p>	<p>Enhanced Terahertz Generation Through Superposition of Beamlets: Theory, Spatial Homogeneity, and Efficiency Analysis</p>	<p>Terahertz Generation Using Superpositions of Beamlets</p>

Figure 9: Generation examples of different models on the title generation task. The red-colored text indicates the content that exists in the ground-truth title, and the green-colored text indicates the content that has not been included in the ground-truth title and abstract.

Title	Ground-truth	Vicuna-13b	GPT-3.5 turbo	LitFM-13b
Adversarial Attacks on Deep Learning Based Power Allocation in a Massive MIMO Network	Deep learning (DL) is becoming popular as a new tool for many applications in wireless communication systems. However, for many classification tasks (e.g., modulation classification) it has been shown that DL-based wireless systems are susceptible to adversarial examples; adversarial examples are well-crafted malicious inputs to the neural network (NN) with the objective to cause erroneous outputs. In this paper, we extend this to regression problems and show that adversarial attacks can break DL-based power allocation in the downlink of a massive multiple-input-multiple-output (maMIMO) network. Specifically, we extend the fast gradient sign method (FGSM), momentum iterative FGSM, and projected gradient descent adversarial attacks in the context of power allocation in a maMIMO system. We benchmark the performance of these attacks and show that with a small perturbation in the input of the NN, the white-box attacks can result in infeasible solutions up to 86%. Furthermore, we investigate the performance of black-box attacks. All the evaluations conducted in this work are based on an open dataset and NN models, which are publicly available.	Deep learning (DL) has emerged as a powerful tool for optimizing power allocation in wireless communication systems, particularly in the context of complex and dynamic environments. However, the vulnerability of DL models to adversarial attacks poses significant challenges to their reliability and security. This paper investigates the impact of adversarial attacks on DL-based power allocation strategies in wireless communication networks. We explore how carefully crafted perturbations can degrade the performance of DL models, leading to suboptimal or even detrimental power allocation decisions. Our study analyzes various types of adversarial attacks, including white-box and black-box attacks, and evaluates their effects on both the accuracy and robustness of DL models in different scenarios. We also discuss potential defense mechanisms to mitigate these attacks and improve the resilience of DL-based power allocation systems. The findings underscore the need for incorporating security considerations into the design of DL algorithms for wireless networks, ensuring that they can operate reliably even in the presence of adversarial threats.	Deep learning (DL) has emerged as a powerful tool for optimizing power allocation in massive multiple-input multiple-output (MIMO) networks, significantly improving network efficiency and performance. However, the deployment of DL models in real-world wireless communication systems presents vulnerabilities to adversarial attacks, which can lead to suboptimal or even catastrophic power allocation decisions. In this paper, we investigate the susceptibility of DL-based power allocation algorithms in massive MIMO networks to adversarial attacks. We explore various attack strategies and demonstrate their effectiveness in disrupting the performance of these algorithms. Our analysis includes both white-box and black-box attack scenarios, highlighting the potential risks posed by adversarially crafted inputs. To mitigate these risks, we propose a set of defense mechanisms designed to enhance the robustness of DL-based power allocation models. Through extensive simulations, we demonstrate that these defenses can significantly reduce the impact of adversarial attacks, ensuring more reliable and secure power allocation in massive MIMO networks. Our findings underscore the importance of considering adversarial threats in the design and deployment of DL-based solutions in wireless communication systems.	Deep learning (DL) is becoming popular as a new tool for many applications in wireless communication systems. However, it is known that DL models are highly sensitive to adversarial attacks. In this paper, we investigate the impact of adversarial attacks on DL-based power allocation in a massive multiple-input-multiple-output (MIMO) network. Firstly, we introduce two types of adversarial attacks, namely white-box attack and black-box attack, and then we formulate them as optimization problems. Secondly, we develop efficient algorithms to solve the formulated problems. Thirdly, we conduct simulations to evaluate the effectiveness of our proposed attacks. Our results indicate that both white-box and black-box attacks can effectively degrade the performance of DL-based power allocation in a massive MIMO network.
Universal Sparse Superposition Codes with Spatial Coupling and GAMP Decoding	Sparse superposition codes, or sparse regression codes, constitute a new class of codes which was first introduced for communication over the additive white Gaussian noise (AWGN) channel. It has been shown that such codes are capacity-achieving over the AWGN channel under optimal maximum-likelihood decoding as well as under various efficient iterative decoding schemes equipped with power allocation or spatially coupled constructions. Here, we generalize the analysis of these codes to a much broader setting that includes all memoryless channels. We show, for a large class of memoryless channels, that spatial coupling allows an efficient decoder, based on the generalized approximate message-passing (GAMP) algorithm, to reach the potential (or Bayes optimal) threshold of the underlying (or uncoupled) code ensemble. Moreover, we argue that spatially coupled sparse superposition codes universally achieve capacity under GAMP decoding by showing, through analytical computations, that the error floor vanishes and the potential threshold tends to capacity as one of the code parameters goes to infinity. Furthermore, we provide a closed form formula for the algorithmic threshold of the underlying code ensemble in terms of a Fisher information. Relating an algorithmic threshold to a Fisher information has theoretical as well as practical importance. Our proof relies on the state evolution analysis and uses the potential method developed in the theory of low-density parity-check (LDPC) codes and compressed sensing.	Sparse superposition codes have gained significant attention in recent years due to their ability to achieve near-optimal performance while maintaining low complexity. These codes are characterized by having a small number of nonzero coefficients, making them well-suited for applications where memory efficiency and computational resources are limited. In this paper, we propose a novel approach to construct universal sparse superposition codes that can be used in various communication scenarios. Our method relies on spatial coupling techniques and generalized approximate message passing (GAMP) decoding to achieve high error correction capabilities. We demonstrate the effectiveness of our proposed codes through simulations and compare them against existing state-of-the-art methods. The results show that our codes outperform other approaches in terms of both performance and complexity, making them an attractive option for practical applications.	Sparse superposition codes (SSC) have emerged as a powerful technique in the realm of communication systems, offering near-optimal performance in various channels. This paper explores the integration of universal sparse superposition codes with spatial coupling and the Generalized Approximate Message Passing (GAMP) algorithm for decoding. Spatial coupling, a technique known to enhance the robustness and efficiency of codes, is combined with SSC to achieve better performance over a wide range of channel conditions. The GAMP decoding algorithm is utilized to decode the spatially coupled SSC, leveraging its computational efficiency and ability to handle large-scale systems. Through both theoretical analysis and simulation, we demonstrate that the proposed system achieves reliable communication at rates approaching the channel capacity, while maintaining computational feasibility. The results suggest that the integration of spatial coupling with SSC, decoded via GAMP, offers a promising approach for future communication systems, particularly in scenarios demanding high reliability and efficiency.	Sparse superposition codes, or sparse regression codes, constitute a new class of codes which was first introduced for communication over the additive white Gaussian noise channel. These codes are now known to be universal, i.e., they achieve capacity over any memoryless channel under generalized approximate message-passing (GAMP) decoding. However, the GAMP decoder has never been explicitly designed for sparse superposition codes. In this work, we propose a novel GAMP decoder for sparse superposition codes, and we analyze its behavior on several channels. Our numerical simulations indicate that the GAMP decoder achieves near-capacity performance on the AWGN channel, while it reach the Bayes optimal on the binary erasure channel. We also demonstrate that the GAMP decoder exhibits a vanishing error floor when the number of nonzero coefficients increases. Finally, we discuss the impact of the choice of the encoding matrix on the performance of the GAMP decoder.
Hybrid Combining Based on Constant Phase Shifters and Active/Inactive Switches	In this paper, we propose a new hybrid analog and digital combining architecture for millimeter wave (mmWave) multi-user multiple-input multiple-output (MU-MIMO) systems. The proposed structure employs antenna subset selection per radio frequency (RF) chain based on active/inactive switches and uses constant phase shifters (CPS) to control the phases of signals in the RF circuit. In this scheme, for each RF chain, a subset of receive antennas that contribute more to the desired signal power than the interference power is chosen for signal combining in the analog domain, whereas other receive antennas are excluded from signal combining, thereby enhancing sum-rates. Simultaneously, the proposed structure reduces power consumption in the RF circuit by exclusively activating switches that correspond to the antennas selected for each RF chain. We also develop three low-complexity algorithms for per-RF chain antenna subset selection. Finally, through numerical simulation, we show that the proposed structure provides higher spectral efficiency and higher energy efficiency than conventional hybrid analog and digital combining schemes for mmWave MU-MIMO systems.	In this paper, we propose a new hybrid analog and digital combining architecture for millimeter wave (mmWave) multi-antenna systems. The proposed architecture employs constant phase shifters and active/inactive switches to achieve efficient power combination while maintaining low complexity. Simulation results demonstrate that our proposed method outperforms existing techniques in terms of both performance and complexity. This work paves the way for practical implementation of high-gain mmWave MIMO systems with reduced hardware requirements.	In this paper, we propose a novel hybrid combining architecture that integrates constant phase shifters with active and inactive switches for millimeter wave (mmWave) multi-user multiple input single output (MISO) systems. This architecture aims to enhance the performance of mmWave communication by leveraging the benefits of both analog and digital combining techniques. The proposed system optimizes beamforming and signal reception through a strategic combination of phase shifting and switching, which improves overall system efficiency and signal quality. Simulation results demonstrate the effectiveness of the hybrid approach in achieving significant gains in signal-to-noise ratio (SNR) and overall system capacity, making it a promising solution for advanced mmWave communication networks.	In this paper, we propose a new hybrid analog and digital combining architecture for millimeter wave (mmWave) multi-user multiple input single output (MISO) systems. The proposed architecture consists of two parts: an active part that uses constant phase shifters to combine the signals from different users at the transmitter side; and an inactive part that uses switches to selectively turn off some of the antennas at the receiver side. We first derive the optimal power allocation strategy based on the maximum ratio transmission (MRT) principle. Then, we analyze the performance of the proposed architecture by deriving closed form expressions for the achievable rate and outage probability. Simulation results show that our proposed architecture can achieve significant gains over conventional architectures with only one type of combining scheme. Moreover, it achieves similar or better performance than the state-of-the-art hybrid analog and digital combining schemes while requiring fewer hardware components.

Figure 10: Generation examples of different models on the abstract completion task. The red-colored text indicates the content that exists in the ground-truth abstract, and the green-colored text indicates the fake information generated by LLM.

Title A	Abstract A	Title B	Abstract B	Ground-truth	Vicuna-13b	GPT-3.5 turbo	LitFM-13b
Observation of higher-order exceptional points in pseudo-Hermitian radio-frequency circuits	Exceptional points (EP) in non-Hermitian systems have been widely investigated due to their enhanced sensitivity in comparison to standard systems. In this letter, we report the observation of higher-order pseudo-Hermitian degeneracies in an electronic platform comprised of three inductively coupled gain-loss LC resonators. Theoretical analysis demonstrates that the proposed system can realize third-order EP with asymmetric coupling between adjacent inductors and an arbitrary scaling factor between two loss resonators. When capacitive perturbation is introduced on the middle resonator, the perturbed eigenfrequencies follow a cube-root dependence on the perturbation parameter; in this case, the sensitivity is significantly greater than conventional wireless readout methods. Our work enriches the explorations of higher-order EP on electronic platforms and provides a new degree of design freedom for the non-Hermitian-EP-enhanced wireless sensing system.	Generalized Parity-Time Symmetry Condition for Enhanced Sensor Telemetry	Wireless sensors based on micro-machined tunable resonators are important in a variety of applications, ranging from medical diagnosis to industrial and environmental monitoring. The sensitivity of these devices is, however, often limited by their low quality (Q) factor. Here, we introduce the concept of isospectral parity time reciprocal scaling (PTX) symmetry and show that it can be used to build a new family of radiofrequency wireless microsensors exhibiting ultrasensitive responses and ultrahigh resolution, which are well beyond the limitations of conventional passive sensors. We show theoretically, and demonstrate experimentally using microelectromechanical based wireless pressure sensors, that PTX-symmetric electronic systems share the same eigenfrequencies as their parity time (PT)-symmetric counterparts, but crucially have different circuit profiles and eigenmodes. This simplifies the electronic circuit design and enables further enhancements to the extrinsic Q factor of the sensors.	Recently, it has been proposed that a PT-symmetry -based wireless sensing system can improve the resolution of the readout spectrum	Recently, Paper A observed higher-order exceptional points in pseudo-Hermitian radio-frequency circuits, which showed enhanced sensitivity in wireless sensing systems	Inspired by the concept of isospectral parity-time reciprocal scaling (PTX) symmetry, as discussed in Paper B), we extend these ideas to demonstrate higher-order exceptional points in pseudo-Hermitian circuits	Recently, several studies have shown that the PT-symmetric systems possess unique properties such as unidirectional transmission, high resolution , and robustness against fabrication errors.
A Data-Driven Statistical-Stochastic Surrogate Modeling Strategy for Complex Nonlinear Non-stationary Dynamics	We propose a statistical-stochastic surrogate modeling approach to predict the response of the mean and variance statistics under various initial conditions and external forcing perturbations. The proposed modeling framework extends the purely statistical modeling approach that is practically limited to the homogeneous statistical regime for high-dimensional state variables. The new closure system allows one to overcome several practical issues that emerge in the non-homogeneous statistical regimes. First, the proposed ensemble modeling that couples the mean statistics and stochastic fluctuations naturally produces positive-definite covariance matrix estimation, which is a challenging issue that hampers the purely statistical modeling approaches. Second, the proposed closure model, which embeds a non-Markovian neural-network model for the unresolved fluxes such that the variance of the dynamics is consistent, overcomes the inherent instability of the stochastic fluctuation dynamics. Effectively, the proposed framework extends the classical stochastic parametric modeling paradigm for the unresolved dynamics to a semi-parametric parameterization with a residual Long-Short-Term-Memory neural network architecture. Third, based on empirical information theory, we provide an efficient and effective training procedure by fitting a loss function that measures the differences between response statistics. Supporting numerical examples are provided with the Lorenz-96 model, a system of ODEs that admits the characteristic of chaotic dynamics with both homogeneous and inhomogeneous statistical regimes. In the latter case, we will see the effectiveness of the statistical prediction even though the resolved Fourier modes corresponding to the leading mean energy and variance spectra do not coincide.	Machine Learning-Based Statistical Closure Models for Turbulent Dynamical Systems	We propose a Machine Learning (ML) non-Markovian closure modeling framework for accurate predictions of statistical responses of turbulent dynamical systems subjected to external forcings. One of the difficulties in this statistical closure problem is the lack of training data, which is a configuration that is not desirable in supervised learning with neural network models. In this study with the 40-dimensional Lorenz-96 model, the shortage of data (in temporal) is due to the stationarity of the statistics beyond the decorrelation time, thus, the only informative content in the training data is on short-time transient statistics. We adopted a unified closure framework on various truncation regimes, including and excluding the detailed dynamical equations for the variances. The closure frameworks employ a Long-Short-Term-Memory architecture to represent the higher-order unresolved statistical feedbacks with careful consideration to account for the intrinsic instability yet producing stable long-time predictions. We found that this unified agnostic ML approach performs well under various truncation scenarios. Numerically, the ML closure model can accurately predict the long-time statistical responses subjected to various time-dependent external forces that are not (and maximum forcing amplitudes that are relatively larger than those) in the training dataset.	Following the work in cite(q2022machine) , we will consider the class of residual network with vanilla LSTM architecture.	In contrast to previous works [1, 2], our proposed statistical-stochastic surrogate modeling strategy effectively addresses the challenges associated with non-homogeneous statistical regimes, as demonstrated through supporting numerical examples with the Lorenz-96 model [3]	Building on the previous work, who proposed a machine learning-based closure modeling framework for turbulent dynamical systems, our study extends the statistical-stochastic surrogate modeling approach to address non-homogeneous statistical regimes and improve covariance matrix estimation.	Following the same strategy as in cite(q2022machine) , we adopt a vanilla LSTM architecture to approximate the unresolved dynamics
PyLab: a cross-platform, open-source inverse modeling toolbox for conventional and Fourier ptychography	Conventional (CP) and Fourier (FP) ptychography have emerged as versatile quantitative phase imaging techniques. While the main application cases for each technique are different, namely lens-less short wavelength imaging for CP and lens-based visible light imaging for FP, both methods share a common algorithmic ground. CP and FP have in part independently evolved to include experimentally robust forward models and inversion techniques. This separation has resulted in a plethora of algorithmic extensions, some of which have not crossed the boundary from one modality to the other. Here, we present an open source, cross-platform software, called PyLab, enabling both CP and FP data analysis in a unified framework. With this framework, we aim to facilitate and accelerate cross-pollination between the two techniques. Moreover, the availability in Matlab, Python, and Julia will set a low barrier to enter each field.	Using Automatic Differentiation as a General Framework for Ptychographic Reconstruction	Coherent diffraction imaging methods enable imaging beyond lens-imposed resolution limits. In these methods, the object can be recovered by minimizing an error metric that quantifies the difference between diffraction patterns as observed, and those calculated from a present guess of the object. Efficient minimization methods require analytical calculation of the derivatives of the error metric, which is not always straightforward. This limits our ability to explore variations of basic imaging approaches. In this paper, we propose to substitute analytical derivative expressions with the automatic differentiation method, whereby we can achieve object reconstruction by specifying only the physics-based experimental forward model. We demonstrate the generality of the proposed method through straightforward object reconstruction for a variety of complex ptychographic experimental models.	Another line of research has investigated the capabilities opened up by modern automatic differentiation (AD) and machine learning (ML) toolboxes cite(Kandel2019) .	Recent development in the field of ptychography is the introduction of PyLab .	PyLab builds on the automatic differentiation methods for ptychographic reconstruction introduced by [1].	Another example of a more recent development is the use of automatic differentiation and machine learning as a general framework for ptychographic reconstruction cite(Kandel2019) .
Model discovery in the sparse sampling regime	To improve the physical understanding and the predictions of complex dynamic systems, such as ocean dynamics and weather predictions, it is of paramount interest to identify interpretable models from coarsely and off-grid sampled observations. In this work, we investigate how deep learning can improve model discovery of partial differential equations when the spacing between sensors is large and the samples are not placed on a grid. We show how leveraging physics-informed neural network interpolation and automatic differentiation, allow to better fit the data and its spatiotemporal derivatives, compared to more classic spline interpolation and numerical differentiation techniques. As a result, deep learning-based model discovery allows to recover the underlying equations, even when sensors are placed further apart than the data's characteristic length scale and in the presence of high noise levels. We illustrate our claims on both synthetic and experimental data sets where combinations of physical processes such as (non-)linear advection, reaction, and diffusion are correctly identified.	SciPy 1.0-Fundamental Algorithms For Scientific Computing in Python	SciPy is an open source scientific computing library for the Python programming language. SciPy 1.0 was released in late 2017, about 16 years after the original version 0.1 release. SciPy has become a de facto standard for leveraging scientific algorithms in the Python programming language, with more than 600 unique code contributors, thousands of dependent packages, over 100,000 dependent repositories, and millions of downloads per year. This includes usage of SciPy in almost half of all machine learning projects on GitHub, and usage by high profile projects including LIGO gravitational wave analysis and creation of the first-ever image of a black hole (M87). The library includes functionality spanning clustering, Fourier transforms, integration, interpolation, file I/O, linear algebra, image processing, orthogonal distance regression, minimization algorithms, signal processing, sparse matrix handling, computational geometry, and statistics. In this work, we provide an overview of the capabilities and development practices of the SciPy library and highlight some recent technical developments.	We would also like to thank the authors and contributors of SciPy cite(scipy) for making our work possible through their open-source software .	We cannot generate a citation sentence because there is no relationship or connection between the two papers	To address the challenges of interpolation and numerical differentiation in the sparse sampling regime, we utilize the SciPy library's advanced interpolation capabilities .	We have implemented the methodology described above in Python using the scipy library cite(scipy)

Figure 11: Generation examples of different models on the citation sentence generation task. The red-colored text indicates the content that exists in the ground-truth abstract, and the green-colored text indicates the fake information generated by LLM.

Title	Abstract	GPI-3.5 turbo	LiFM-13b	Title of cited papers
current strategy to treat immunogenic gastrointestinal cancers perspectives for a new era	Since pembrolizumab, an anti-programmed death-1 (PD-1) antibody, showed a dramatic response to immunogenic cancers with microsatellite instability-high (MSI-H) and/or deficient mismatch repair (dMMR) in the pilot clinical trial KEYNOTE-016, subsequent studies have confirmed durable responses of anti-PD-1 inhibitors for MSI-H/dMMR solid tumors. As immunotherapy is described as a "game changer", the therapeutic landscape for MSI-H/dMMR solid tumors including gastrointestinal cancers has changed considerably in the last decade. An MSI/MMR status has been established as the predictive biomarker for immune checkpoint blockade, playing an indispensable role in the clinical practice of patients with MSI-H/dMMR tumors. Immunotherapy is also now investigated for locally advanced MSI-H/dMMR gastrointestinal cancers. Herein, we review recent clinical trials with special attention to MSI-H/dMMR gastrointestinal cancers together with basic/translational findings, which provide their rationale, and discuss perspectives for the further therapeutic development of treatment in this field.	The advent of immunotherapy, particularly with the use of immune checkpoint inhibitors like pembrolizumab, has revolutionized the treatment of immunogenic cancers, especially those with microsatellite instability-high (MSI-H) and deficient mismatch repair (dMMR) status. The pivotal KEYNOTE-016 trial (Le et al., 2015) demonstrated the remarkable efficacy of pembrolizumab in MSI-H/dMMR cancers, setting the stage for subsequent studies that have consistently confirmed durable responses across various solid tumors, including gastrointestinal cancers. Several studies have since established MSI/MMR status as a crucial biomarker for predicting responses to immune checkpoint blockade (Overman et al., 2017). The significance of this biomarker has been underscored by its incorporation into routine clinical practice, where it guides therapeutic decisions in treating MSI-H/dMMR tumors (Cohen et al., 2017). Furthermore, the exploration of immunotherapy for locally advanced MSI-H/dMMR gastrointestinal cancers has opened new avenues for treatment, with ongoing trials investigating the expansion of these approaches (André et al., 2020). However, despite the successes, not all patients with MSI-H/dMMR gastrointestinal cancers respond to immunotherapy, a challenge that has been attributed to the presence of intrinsic or acquired resistance mechanisms. Recent research has focused on understanding these resistance mechanisms, with several studies exploring combination therapies and novel agents to enhance the efficacy of immunotherapy in these populations (Diaz et al., 2017; Le et al., 2020). The ongoing efforts to overcome resistance highlight the need for continued investigation into the molecular underpinnings of resistance and the development of next-generation therapeutic strategies. Andro, T., Shiu, K. K., Kim, T. W., Jensen, B. V., Jensen, L. H., Punt, C., ... & Tabernero, J. (2020). Pembrolizumab in microsatellite- <i>instability</i> -high advanced colorectal cancer. <i>New England Journal of Medicine</i> , 383(23), 2207-2218. Cohen, R., Bahard, O., Corvera, P., Hain, E., Dumont, S., Bardier, A., ... & Svrcek, M. (2017). Clinical and molecular characterization of mismatch repair proficient, methylation-low colorectal cancer: a multi-institutional study. <i>British Journal of Cancer</i> , 116(12), 1630-1639. Diaz, L. A., Le, D. T., & Mertens, L. (2017). Mismatch repair deficiency as a predictive biomarker for immunotherapy in cancer: a review. <i>JAMA Oncology</i> , 3(4), 380-386. Le, D. T., Durham, J. N., Smith, K. N., Wang, H., Bartlett, B. R., Aulakh, L. K., ... & Diaz, L. A. (2015). Mismatch repair deficiency predicts response of solid tumors to PD-1 blockade. <i>Science</i> , 348(6230), 233-240. Le, D. T., Kim, T. W., Van Cutsem, E., Geva, R., Jäger, D., Hara, H., ... & Overman, M. J. (2020). Phase II open-label study of pembrolizumab in patients with advanced microsatellite <i>instability</i> -high/mismatch repair-deficient solid tumors. <i>KEYNOTE-164</i> . <i>Journal of Clinical Oncology</i> , 38(1), 1-10. Overman, M. J., McDermott, R., Leach, J. L., Lonardi, S., Lenz, H. J., Morse, M. A., ... & Kopetz, S. (2017). Nivolumab in patients with metastatic DNA mismatch repair-deficient or microsatellite <i>instability</i> -high colorectal cancer (CheckMate 142): an open-label, multicentre, phase 2 study. <i>The Lancet Oncology</i> , 18(9), 1182-1191.	Recent studies have focused on improving our understanding of the role of immune checkpoints in cancer and developing strategies to overcome them [1]. The use of biomarkers such as tumor mutational burden (TMB) has shown promise in identifying patients who may respond well to immunotherapy [1, 12]. Other research has examined the relationship between microsatellite instability (MSI) and immune checkpoint inhibitors, finding that MSI-high cancers tend to have better outcomes when treated with these drugs [2, 13]. Additionally, combining immune checkpoint blockade with traditional cytotoxic agents has shown promising results in clinical trials for various cancer types, particularly in MSI-high solid tumors [3, 14]. Several studies have explored the potential of biomarkers such as programmed death ligand 1 (PD-L1) and chromosomal instability (CIN) in predicting the immunogenicity of tumors [4, 5, 11]. Others have investigated the impact of Jak-STAT signaling pathway alterations on immune response and neoantigen presentation in tumor cells [6]. Furthermore, research has focused on identifying additional biomarkers for predicting response to immunotherapy, including mutations in beta 2 microglobulin and homologous recombination deficiency [7, 8]. Combinatorial approaches involving multiple immune checkpoint inhibitors have also been studied, particularly in MSI-high solid tumors [9, 10]. Anticipating the benefits of these strategies beyond the MSI status, recent clinical trials have explored the use of immune checkpoint blockade in various cancer types [10, 15]. Overall, these studies highlight the importance of understanding the complex interplay between the immune system and cancer, and the need for personalized treatment approaches based on individual patient characteristics.	1. Association of tumour mutational burden with outcomes in patients with advanced solid tumours treated with pembrolizumab: prospective biomarker analysis of the multicohort, open-label, phase 3 KEYNOTE-158 study. 2. Hallmarks of cancer: the next generation. 3. Mismatch repair deficiency predicts response of solid tumors to PD-1 blockade. 4. PD-1 Blockade in Tumors with Mismatch-Repair Deficiency. 5. Comprehensive molecular characterization of human colon and rectal cancer. 6. Tumour-intrinsic resistance to immune checkpoint blockade. 7. Tumor Mutational Burden as an Independent Predictor of Response to Immunotherapy in Diverse Cancers. 8. Signatures of mutational processes in human cancer. 9. Pembrolizumab for the treatment of non-small-cell lung cancer. 10. First-line nivolumab plus chemotherapy versus chemotherapy alone for advanced gastric, gastro-oesophageal junction, and oesophageal adenocarcinoma (CheckMate 649): a randomised, open-label, phase 3 trial. 11. Immunogenic cell death in cancer and infectious disease. 12. Oncology meets immunology: the cancer-immunity cycle. 13. Cancer Immune Evasion Through Loss of MHC Class I Antigen Presentation. 14. Clinical Sequencing Defines the Genomic Landscape of Metastatic Colorectal Cancer. 15. First-line nivolumab plus ipilimumab combined with two cycles of chemotherapy in patients with non-small-cell lung cancer (CheckMate 91A): an international, randomised, open-label, phase 3 trial. 16. Relatlimab and Nivolumab versus Nivolumab in Untreated Advanced Melanoma.
multi-omic longitudinal study reveals immune correlates of clinical course among hospitalized COVID-19 patients	The IMPACC cohort, composed of >1,000 hospitalized COVID-19 patients, contains five illness trajectory groups (TGs) during acute infection (first 28 days), ranging from milder (TG1-3) to more severe disease course (TG4) and death (TG5). Here, we report deep immunophenotyping, profiling of >15,000 longitudinal blood and nasal samples from 540 participants of the IMPACC cohort, using 14 distinct assays. These unbiased analyses identify cellular and molecular signatures present within 72 h of hospital admission that distinguish moderately from severe and fatal COVID-19 disease. Importantly, cellular and molecular states also distinguish participants with more severe disease that recover or stabilize within 28 days from those that progress to fatal outcomes (TG4 vs. TG5). Furthermore, our longitudinal design reveals that these biologic states display distinct temporal patterns associated with clinical outcomes. Characterizing host immune responses in relation to heterogeneity in disease course may inform clinical prognosis and opportunities for intervention.	The study of immune responses in COVID-19 has been pivotal in understanding the heterogeneity of disease outcomes. Previous research has primarily focused on cross-sectional analyses of immune profiles in patients with varying severity of COVID-19. For example, Mathew et al. (2020) identified distinct immune signatures associated with mild, moderate, and severe COVID-19 cases, highlighting the role of specific immune cell populations in disease progression. Similarly, Arnschelm et al. (2021) characterized cytokine and chemokine responses in severe COVID-19, emphasizing the role of hyperinflammation in adverse outcomes. Longitudinal studies have provided deeper insights into the dynamics of immune responses over the course of infection. Lucas et al. (2021) conducted a longitudinal immune profiling study that revealed the temporal evolution of immune markers associated with disease severity, offering a more nuanced understanding of how immune responses correlate with clinical outcomes. Additionally, Su et al. (2020) utilized multi-omic approaches to explore the interplay between the host and the biological systems, providing a holistic view of the host response to SARS-CoV-2 infection. Despite these advances, the integration of multi-omic data across large cohorts, such as the IMPACC cohort, remains relatively unexplored. The use of multi-omic approaches in longitudinal studies enables the identification of early biomarkers and the tracking of immune trajectories, offering potential for predictive modeling of disease progression. Our study builds on these foundational works by employing a comprehensive, multi-omic approach across a large cohort of hospitalized COVID-19 patients, capturing the complexity of immune responses and their association with clinical outcomes over time.	Several studies have investigated the immune correlates of COVID-19, focusing on various aspects such as cytokine profiles, immune cell populations, and transcriptional changes. For example, a study analyzed cytokine and chemokine expression in COVID-19 patients and found increased activators of cytotoxic natural killer cells, including IL-12B and CD244 [3]. Another study examined the relationship between clinical trajectories and transcriptomic modules in COVID-19 patients and identified several modules with significant differences in expression levels between trajectory groups [15]. Moreover, a study utilizing Olink proteomics measured inflammatory biomarkers, including IL-6, and found a clear association between resolution of inflammation in 28-day survivors versus non-survivors [11]. Additionally, a study investigated the proinflammatory role of the TNF signaling pathway in COVID-19 mortality, linking it to inflammatory cell death induced by TNF and IFN-γ signaling [15]. In recent years, there has been growing interest in using single-cell technologies to dissect the heterogeneity within immune cell populations. Single-cell RNA sequencing (scRNA-Seq) has been employed to identify distinct subpopulations of immune cells and understand their functions during different stages of infections and diseases. For example, a study applied scRNA-Seq to investigate the dynamics of immune responses in SARS-CoV-2 infected patients, identifying unique T cell subsets with distinct transcriptional signatures [6]. Similarly, another study used scRNA-Seq to analyze immune cell populations in COVID-19 patients and discovered novel T cell states characterized by distinct transcriptional programs [7]. Furthermore, a study utilized scRNA-Seq to analyze T cell responses in COVID-19 patients and revealed distinct T cell subsets with distinct gene expression patterns [8].	1. High concentration of branched-chain amino acids promotes oxidative stress, inflammation and migration of human peripheral blood mononuclear cells via mTORC1 activation. 2. STAR: ultrafast Illumina-raw-seq aligner. 3. Profiling serum cytokines in COVID-19 patients reveals IL-6 and IL-10 as disease severity predictors. 4. Molecular and cellular insights into T cell exhaustion. 5. Fast gapped-read alignment with Bowtie 2. 6. MetaB-Analyst 10: narrowing the gap between raw spectra and functional insights. 7. Clinical Characteristics of Coronavirus Disease 2019 in China. 8. Skyline: an open source document editor for creating and analyzing targeted proteomics experiments. 9. KEGG as a reference resource for gene and protein annotation. 10. The STRING database in 2021: customizable protein-protein networks and functional characterization of user-uploaded gene measurement sets. 11. HISEq-a Python framework to work with high-throughput sequencing data. 12. An inflammatory cytokine signature predicts COVID-19 severity and survival. 13. Trimmomatic: a flexible trimmer for Illumina sequence data. 14. Clinical features of patients infected with 2019 novel coronavirus in Wuhan, China. 15. Synergism of TNF-α and IFN-γ Triggers Inflammatory Cell Death, Tissue Damage, and Mortality in SARS-CoV-2 Infection and Cytokine Shock Syndromes. 16. The Molecular Signatures Database (MSigDB) hallmark gene set collection. 17. PLINK: a tool set for whole-genome association and population-based linkage analyses. 18. The Sequence Alignment/Map format and SAMtools.
Massive Access in Secure NOMA under Imperfect CSI: Security Guaranteed Sum-Rate Maximization with First-Order Algorithm	Non-orthogonal multiple access (NOMA) is a promising solution for secure transmission under massive access. However, in addition to the uncertain channel state information (CSI) of the eavesdroppers due to their passive nature, the CSI of the legitimate users may also be imperfect at the base station due to the limited feedback. Under both channel uncertainties, the optimal power allocation and transmission rate design for a secure NOMA scheme is currently not known due to the difficulty of handling the probabilistic constraints. This article fills this gap by proposing novel transformation of the probabilistic constraints and variable decoupling so that the security guaranteed sum-rate maximization problem can be solved by alternatively exploiting branch-and-bound method and difference of convex programming. To scale the solution to a truly massive access scenario, a first-order algorithm with very low complexity is further proposed. Simulation results show that the proposed first-order algorithm achieves identical performance to the conventional method but saves at least two orders of magnitude in computation time. Moreover, the resultant transmission scheme significantly improves the security guaranteed sum-rate compared to the orthogonal multiple access transmission and NOMA ignoring CSI uncertainty.	Massive access scenarios in wireless communication systems have posed significant challenges, particularly in the context of secure transmissions. Non-orthogonal multiple access (NOMA) has emerged as a key enabler for efficient spectrum utilization and enhanced connectivity in such scenarios (Ding et al., 2017). NOMA allows multiple users to share the same frequency resources by superimposing their signals, thereby improving spectral efficiency. However, ensuring security in NOMA systems, especially under imperfect channel state information (CSI), remains a critical challenge. Existing research has addressed various aspects of NOMA in secure communication. For instance, Wang et al. (2018) analyzed secure transmission strategies in NOMA under perfect CSI, demonstrating the potential of NOMA to enhance secrecy capacity compared to orthogonal multiple access (OMA) schemes. However, these works often assume perfect CSI, which is impractical in real-world scenarios where CSI is typically imperfect due to estimation errors or feedback delays (Zhang et al., 2019). In response to these limitations, several studies have explored robust power allocation and beamforming strategies for secure NOMA with imperfect CSI. For example, Liu et al. (2020) proposed a robust beamforming approach that considers CSI uncertainties to maximize the secrecy rate in NOMA systems. Nonetheless, these approaches generally involve complex optimization problems, which are computationally intensive and may not scale well in massive access scenarios. To address the scalability issue, first-order algorithms have gained attention for their ability to provide near-optimal solutions with significantly reduced computational complexity. Huang et al. (2021) introduced a first-order method for large-scale optimization in NOMA, ensuring energy efficiency. However, the application of first-order algorithms to security-constrained sum-rate maximization in NOMA under imperfect CSI remains underexplored. This paper contributes to this research gap by introducing a novel approach that transforms the probabilistic constraints and decouples variables, enabling the use of a low-complexity first-order algorithm to solve the security-guaranteed sum-rate maximization problem in NOMA under both legitimate and eavesdropper CSI uncertainties.	Non-orthogonal multiple access (NOMA) has been recognized as a promising solution for secure transmission under massive access [1][2]. However, the use of NOMA in practice faces challenges such as the uncertainty of channel state information (CSI), which affects the performance of the system [3]. In particular, the CSI of the legitimate users may be imperfect due to the limited feedback at the base station [5], while the CSI of the eavesdroppers remains unknown due to their passive nature [6]. As a result, the optimal power allocation and transmission rate design for a secure NOMA scheme remain unclear due to the difficulty of handling the probabilistic constraints [7]. To address this challenge, several research efforts have focused on developing algorithms to solve the security-guaranteed sum-rate maximization problem in NOMA systems with imperfect CSI [8][9][10]. One approach is to employ zero-forcing beamforming to suppress interference among clusters [11]. Another strategy is to apply successive interference cancellation (SIC) within each cluster to improve the system performance [12]. These techniques aim to enhance the security and efficiency of NOMA-based communication systems. In this context, our paper contributes to the literature by proposing a novel approach that transforms the probabilistic constraints and decouples variables, enabling the use of a low-complexity first-order algorithm to solve the security-guaranteed sum-rate maximization problem in NOMA systems with imperfect CSI using branch-and-bound method and difference of convex programming [13]. Our proposed algorithm has a low computational complexity, making it suitable for large-scale deployment. The simulation results demonstrate that our proposed scheme significantly improves the security-guaranteed sum-rate compared to the orthogonal multiple access transmission and NOMA without considering the CSI uncertainty [14].	1. Securing Downlink Massive MIMO-NOMA Networks with Artificial Noise 2. Edge-Assisted V2X Motion Planning and Power Control Under Channel Uncertainty 3. Beamforming Design and Power Allocation for Secure Transmission with NOMA 4. Massive Connectivity with Massive MIMO-Part I: Device Activity Detection and Channel Estimation 5. On the Performance Gain of NOMA over OMA in Uplink Communication Systems 6. Secure Communications in a Unified Non-Orthogonal Multiple Access Framework 7. Practical Non-linear Energy Harvesting Model and Resource Allocation for SWIPT Systems 8. Robust and Secure Resource Allocation for Full-Duplex MIMO Multicarrier NOMA Systems 9. Prospective Multiple Antenna Technologies for Beyond 5G 10. Downlink SDMA with Limited Feedback in Interference-Limited Wireless Networks 11. Optimal Resource Allocation for Power-Efficient MC-NOMA with Imperfect Channel State Information 12. A Survey of Physical Layer Security Techniques for 5G Wireless Networks and Challenges Ahead 13. Exploiting Inter-User Interference for Secure Massive Non-Orthogonal Multiple Access 14. Secure Users Oriented Downlink MISO NOMA
		Ding, Z., Adachi, F., & Poor, H. V. (2017). The application of non-orthogonal multiple access in LTE and 5G. <i>IEEE Communications Magazine</i> , 55(2), 185-191. Wang, P., Zhu, Y., & Liang, Y. (2018). Secrecy capacity optimization for NOMA with perfect CSI. <i>IEEE Transactions on Communications</i> , 66(9), 3983-3996. Zhang, R., Chen, W., & Huang, Y. (2019). Secure transmission in NOMA systems with imperfect CSI. <i>IEEE Transactions on Vehicular Technology</i> , 68(10), 9869-9873. Liu, L., Zhang, J., & Ma, X. (2020). Robust beamforming for secure NOMA with imperfect CSI. <i>IEEE Transactions on Wireless Communications</i> , 19(4), 2698-2710. Huang, Q., Wang, J., & Yang, J. (2021). First-order methods for energy-efficient NOMA systems. <i>IEEE Transactions on Green Communications and Networking</i> , 5(2), 655-667.		

Figure 12: Generation examples of different models on the related work generation task. The green-colored text indicates the fake citations that do not exist.